

TSHD Trail Force Estimation

MASTER OF SCIENCE THESIS



BRAM VAN DEN BERG

TU Delft - Faculty of 3ME
Delft Center for System and Control
Supervisor: prof. dr. R. Babuska

Royal IHC - IHC Systems
R&D Department
Supervisor: ir. P.M. van den Bergh



TSHD Trail Force Estimation

MASTER OF SCIENCE THESIS

For the degree of Master of Science in Mechanical Engineering at
Delft University of Technology

Bram van den Berg

September 27, 2016

Faculty of Mechanical, Maritime and Materials Engineering (3mE) · Delft
University of Technology

Summary

A trailing suction hopper dredger (TSHD) is a dredging vessel used for harbor and waterway maintenance and sand delivery for land reclamation. The TSHD trails a draghead over the bottom that has to break the coherence of the soil. The loosened soil is sucked up with the dredge pump and transported via the suction mouth and pipe line system into the hopper. The excavation process results in a trail force acting on the draghead and the ship which influences the ship motion significantly.

For optimal ship positioning, optimal draghead control and minimal power consumption, the actual trail force and current are important to know for the dredge operator or automation system. With the trail force and current, the disturbances are counteracted by adjusting the propellers and rudders of the ship. Measuring the trail force is possible, but expensive and vulnerable, therefore an estimator is built to estimate the trail force. The currently used estimator can be improved since more knowledge about the dredging processes is now available. Furthermore, the modern dragheads and suction tubes are equipped with more sensors which are available for the estimator.

Models describing the processes in the draghead and the motion of the ship are built and validated with measurement data. The models are used to construct the estimator. Since the processes contain nonlinearities, the estimator uses the unscented Kalman filter algorithm. First, the trail force is modelled using measurements from the draghead and suction pipe. By combining this information with a ship model and measurements from the GPS and the ships actuators, an estimation of the current and the trail force is made. The estimator must cope with the ever-varying dredging circumstances such as the soil type and dredging depth and with model and measurement uncertainties.

The estimator is tested on simulations from a modelled TSHD. Therefore, a test scenario was defined that represents realistic dredging circumstances. It is shown that the trail force and current are estimated accurately. The trail force estimation has a VAF of 99% and a steady state error of 2%. Especially the slow dynamics are estimated accurately. The currently used method is simulated as well and achieves a VAF of 95%. Therefore, an improvement using the trail force model for the estimator is shown. The current estimation converges as well and contains a steady state error of 0.1 m/s. Measurement data from a seatrial is also used to test the estimator. It is shown that the estimator works as well. However, it is much harder to measure the performance of the estimator with this data. The reliability of the trail force measurements is limited and not all signals were available to model the trail force on the starboard side.

This thesis shows an improvement using the trail force model for the estimator. It is therefore expected that implementing this method on TSHD's will improve their performance. However, it is recommended to fall back on the currently used method when the visor cylinders are at their minimum or maximum position since then the trail force model is not valid. Furthermore, the trail force model can be improved with further research on bulldozing, since this is considered to be the main cause for inaccuracies of the trail force model.



IHC Systems B.V.



Technische Universiteit Delft

EMBARGO

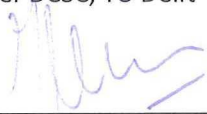
Op het afstudeerverslag getiteld:

“TSHD Trail Force Estimation”

De “Faculteit Werktuigbouwkunde, Maritieme Techniek & Technische Materiaalwetenschappen” van de “Technische Universiteit Delft” zal het afstudeerverslag tot 5 jaar na de afstudeerdatum niet aan derden verstrekken of ter inzage geven zonder toestemming van IHC Systems B.V., gevestigd te Sliedrecht, Industrieweg 30, 3361 HJ.

De afstudeerder, beoordelaar(s) van IHC Systems en namens de Technische Universiteit Delft de betrokken afdelingsvoorzitter(s) verklaren bij deze het embargo te zullen eerbiedigen en de inhoud van het afstudeerverslag strikt vertrouwelijk te behandelen voor de genoemde periode.

Aldus in meervoud opgemaakt en ondertekend,

Te Sliedrecht, d.d. 10 juni 2016 B. van den Berg Afstudeerder Handtekening: 	Te Delft, d.d. 10 juni 2016 Prof.dr.ir. J. Hellendoorn Afdelingsvoorzitter DCSC, TU Delft Handtekening: 
Te Sliedrecht, d.d. 10 juni 2016 Ir. P.M. van den Bergh Beoordelaar IHC Systems Handtekening: 	Te Sliedrecht, d.d. 10 juni 2016 Ir. J. Osnabrugge Beoordelaar IHC Systems Handtekening: 

Contents

Summary	1
1 Introduction	5
1.1 The TSHD	6
1.2 Problem description	6
1.3 Outline of this thesis	7
2 TSHD dredging process	8
2.1 Ship motion	8
2.2 Excavation process	10
2.2.1 The dredging cycle	10
2.2.2 Draghead	12
2.3 Trail force and ship motion control	14
3 Modelling the ship dynamics and the trail force	16
3.1 Ship dynamics	16
3.1.1 Accelerations	18
3.1.2 Propeller	18
3.1.3 Rudder	21
3.1.4 Drag force	22
3.1.5 Pipe forces	24
3.1.6 Bow thrusters	25
3.1.7 Conclusion	25
3.2 Trail force	26
3.2.1 Visor	27
3.2.2 Lower tube	30
3.2.3 Validation	33
4 Estimator design	35
4.1 The unscented Kalman filter	36
4.2 One dimensional estimator	39
4.2.1 State equations	39
4.2.2 Working principle	40
4.3 Two dimensional estimator with current	41
4.4 Summary	44
5 Estimation results	45
5.1 Estimating using simulation data	46
5.1.1 Scenario	46
5.1.2 Estimation results on simulations	51
5.1.3 Comparing the results with the benchmark	54
5.2 Estimating using measurement data from seatrial	56
5.2.1 Scenario	56
5.2.2 Estimation results on measurements	57

6	Conclusions and Recommendations	61
6.1	Conclusions	61
6.2	Recommendations	62
A	Simulink model	64
A.1	Ship model	65
A.2	Excavation model	66
A.3	Estimator model	67
B	Matlab scripts	68
B.1	Trail force modelling	68
B.2	UKF algorithm	69
B.3	State equations for one dimensional estimator	71
B.4	State equations for two dimensional estimator with current	72
C	Cutting force angle	74

Chapter 1

Introduction

Ship transport is the largest carrier of cargo for many centuries. To make transport by water possible for larger ships, waterways have to be kept at a certain depth. Canals, harbors and especially deltas, where sedimentation is high, have to be maintained periodically to guarantee the accessibility.

Around intensively used regions with a shortage of space, claiming land from the sea is a solution. Well-known examples are the airport of Hong Kong, which is built on an artificial island of 940 hectares in sea [?], or the several islands of Dubai like The World (940 hectares) and Palm Jumeirah (650 hectares). The Maasvlakte in Rotterdam was created in the 1960s to provide extra space for the harbor and its industry. After an expansion in 2013 - "Maasvlakte 2", it has grown from 2000 to 5000 hectares. With the expansion, the harbor of Rotterdam tries to maintain the leading position of Europe. In 2025 the Maasvlakte 2 is planned to be completely operational. An impression of this is shown below in Figure 1.1.



Figure 1.1: Impression of the Maasvlakte in Rotterdam in 2025, source: [?]

To make the maintenance and huge land reclamation projects possible, dredging is needed. Large scale dredging is mostly done using cutter suction dredgers and trailing suction hopper dredgers.

The cutter suction dredgers are equipped with cutter heads and are used for rigid soil. The trailing suction hopper dredgers are equipped with dragheads and are used for loose soil, and this is where this thesis focuses on. This thesis is commissioned by IHC-Systems.

1.1 The TSHD

The TSHD trails a draghead along a trajectory on the soil. The draghead excavates sand from the bottom using teeth and jets, which causes a trail force on the draghead. To counteract for this resistance, the required thrust force of the TSHD increases significantly. A mixture of water and sand excavated from the draghead is pumped up by the dredge pump and then transported to the hopper with the suction pipe. The sand settles and water flows overboard until the hopper is filled with sand. A schematic drawing is shown in Figure 1.2.

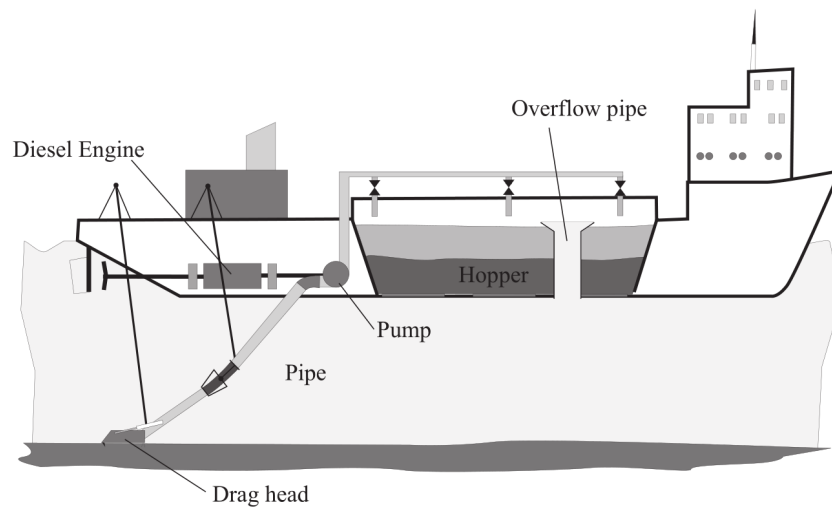


Figure 1.2: Schematic drawing of a TSHD, source: [?]

After sailing to another location, the sand is unloaded using bottom doors or by using the dredge pump again. It is pumped ashore or blown on an area ('rainbowing'). During operation, the position and motion of the TSHD is regulated by the dynamic positioning system.

The dynamic positioning system (DP-system) controls the position or trajectory of the ship which is required to perform the dredging or unloading operation. The high-level controller directs the main propellers, rudders and bow thruster to deliver the desired forces. The low-level controllers will then ensure these desired forces by adjusting the propellers, rudders and bow thruster. This is explained by Sørensen [?]. The DP-system needs to correct for disturbances like wind, current and trail force, since these affect the motion of the ship significantly. Only when the velocity of the ship is controlled well, the dredging process can be optimised and time and fuel is saved.

1.2 Problem description

The wind is measured, but the current and trail force are hard to monitor with a robust method. Currently, the DP-systems of IHC have an estimate about the trail force of the draghead available. This estimate is based on the pressure in the draghead. The current of the water is considered to be an unknown disturbance. The position and velocity of the ship can be controlled more accurately if more is known about these influences, since they affect the ship motion significantly. With the disturbances known, the DP-system will be able to handle them using feed-forward control, even when the ship motion or dredge situation changes.

Furthermore, if more detailed information is available about the dredging process, the draghead can be controlled better to improve the fuel and dredging efficiency of the ship as well. It is possible to measure the trail force using force sensors at the suction pipe. However, this is expensive and fragile because of the rough circumstances. Since the availability of the sensor is not guaranteed, this is not a robust solution and an estimator is desired. The structure of the control loop with the estimated disturbances included is shown in Figure 1.3.

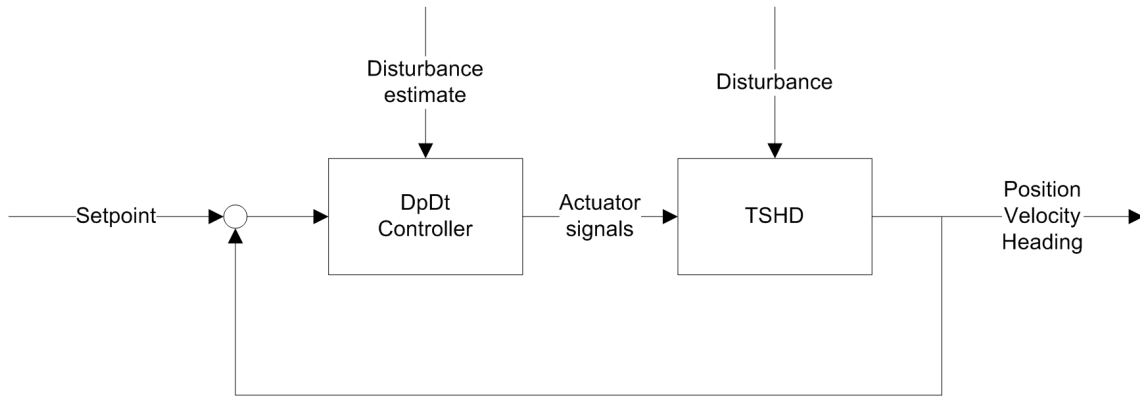


Figure 1.3: Scheme of the DpDt controlled TSHD

The ship's automation system manages all motion and dredge functions. The exported actions are based on measurements, prediction models and objectives. It is desired to maximise the dredging production and efficiency. The DP-system has to ensure that the ship stays at an optimal constant velocity to achieve this, since the dredging efficiency can then be optimised. Controlling the velocity is a challenge, because the circumstances change continuously and the measurements and models have a limited reliability. It is expected that augmenting the DP-system with more refined estimations of the trail force and the current will improve the accuracy of the ship's motion. The estimations will be based on measurements and models from multiple processes on the ship. To build an estimator, a model of the processes and a filter technique is needed. Therefore, both of these subjects will be investigated in this thesis.

1.3 Outline of this thesis

In this thesis it is investigated how the trail force and the current can be estimated. Chapter 2 describes the functioning of the TSHD as a whole and the excavation process in the draghead. This information is needed so the models of the TSHD and the draghead can be specified, which is done in Chapter 3. Model parts are worked out that can be used to build the trail force estimator. Chapter 4 describes how the estimator is built and the working principle is shown as well. The estimator is then applied on simulations and on measurement data. This is explained in Chapter 5. Conclusions and recommendations for further research are made in the last chapter.

Chapter 2

TSHD dredging process

In this chapter, the dredging process of the TSHD is described. An overview of the motion of the ship is given in Section 2.1. Then in Section 2.2, the dredging cycle is explained, together with the working principle and the parts of the draghead. Finally, the dynamic positioning and dynamic tracking system is treated in Section 2.3.

2.1 Ship motion

Several configurations of a TSHD are possible. It is often powered with two diesel engines. These engines power generators which provide electricity for bow thrusters, one or more jet pumps, the hydraulics and other consumers. The propellers and the dredge pump are either driven with electric motors or directly with the diesel engine. With the use of an electric motor it is easier to adjust to the desired speed of rotation, but this configuration is more expensive than a directly driven configuration. An example of a layout with directly driven propellers and dredge pump is shown in Figure 2.1.

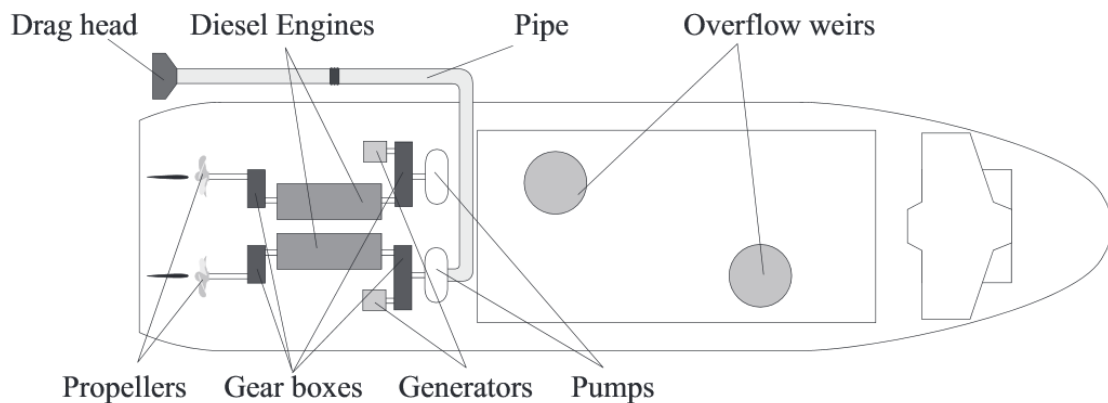


Figure 2.1: A layout of the TSHD, source: [?]

If the propellers are directly driven by the diesel engine, they will often have an adjustable pitch angle. These controllable pitch propellers (CPP) are able to provide the desired thrust force at a fixed engine speed. In Figure 2.2, a CPP of the TSHD 'Congo River' is shown. A rudder behind the propeller enables the ship to steer. A ship with two propellers also has the ability to steer by applying different thrust forces on the propellers.



Figure 2.2: Controllable pitch propellers and rudders of the Congo River, source: [?]

To improve the maneuverability of the ship, bow thrusters are placed at the front of the ship. Using them also improves the ability of keeping track while dredging. Especially if only 1 draghead is trailed along the ship, bow thrusters are helpful to counteract the large momentum acting on the ship. Bow thrusters are only effective for low velocities, so mainly while dredging. At higher velocities, the combination of propeller and rudder is a better option to steer according to [?].

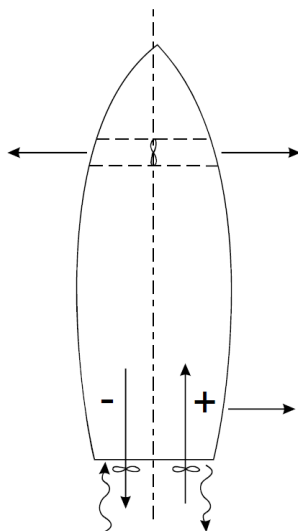


Figure 2.3: Transverse motion using bow thrusters and opposite screws, source: [?]

In Figure 2.3 it is shown how a sideways motion can be performed if the ship is equipped with bow thrusters and two propellers. Because a motion like this is possible with bow thrusters, they improve the manoeuvrability.

The ship and the draghead are desired to track a certain trajectory. Because of disturbances like wind, current and trail force, this can be a challenge. The current is slowly varying which will make it possible to estimate accurately. The trail force is a more varying disturbance because of the uneven bottom and changing soil properties. With these disturbances known, the required propulsion forces can be determined to counteract for. When the dredging process or ship motion changes, the estimation of the disturbances is then adjusted directly.

2.2 Excavation process

2.2.1 The dredging cycle

The dredging cycle of the TSHD includes the excavating, loading and unloading of the soil. When the ship has reached the dredge destination, the ship speed is reduced to approximately 2 knots (about 1 m/s). The draghead is lowered to the bottom and the dredge pump is engaged. The draghead trails along the bottom and excavates soil using its jets and teeth. A water-sand mixture is pumped through the pipe system into the hopper of the TSHD. The suction pipe and the draghead are positioned with winches and cables as shown in Figure 2.4.

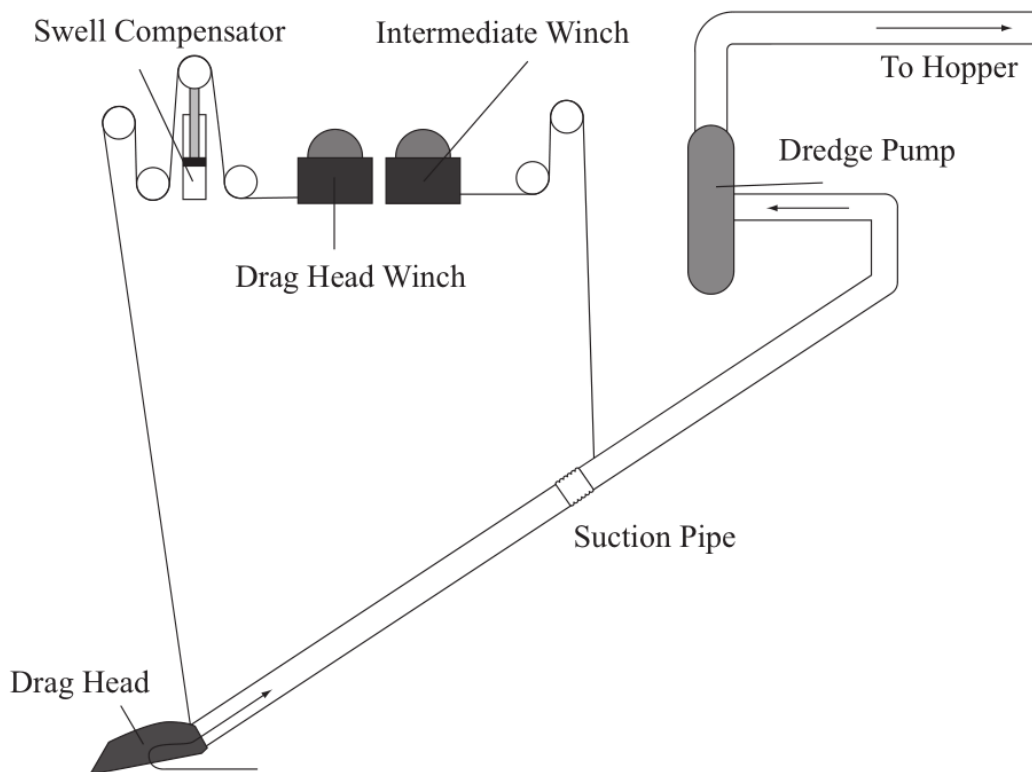


Figure 2.4: The excavation system of the TSHD, source: [?]

A swell compensator counteracts for height differences between the ship and the bottom, resulting from an uneven bottom and waves. By using a pressure vessel with hydraulic oil, it is ensured that the draghead touches the bottom with a constant force. In Figure 2.5, a photo of the swell compensator is shown together with a schematic drawing.

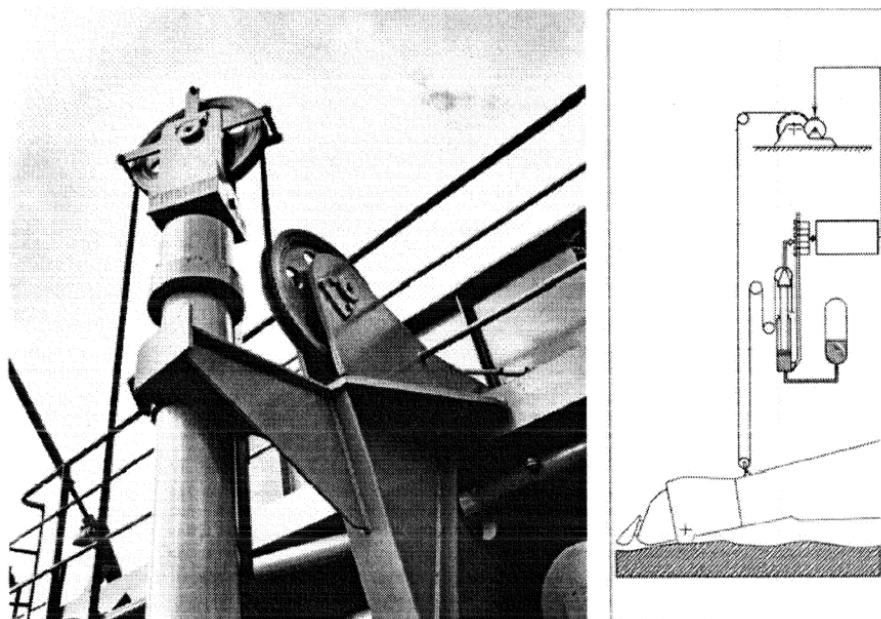


Figure 2.5: The swell compensator, source: [?]

The water-sand mixture from the suction pipe is pumped into the hopper. The sand settles and the water is transported overboard using adjustable overflow pipes. When the hopper is filled with sand, the draghead is hoisted and the ship sails to the discharge location. This is shown in Figure 2.6.



Figure 2.6: The suction pipe hoisted with gantries, source: [?]

A TSHD is able to unload the sand in several ways. These are illustrated in Figure 2.7.

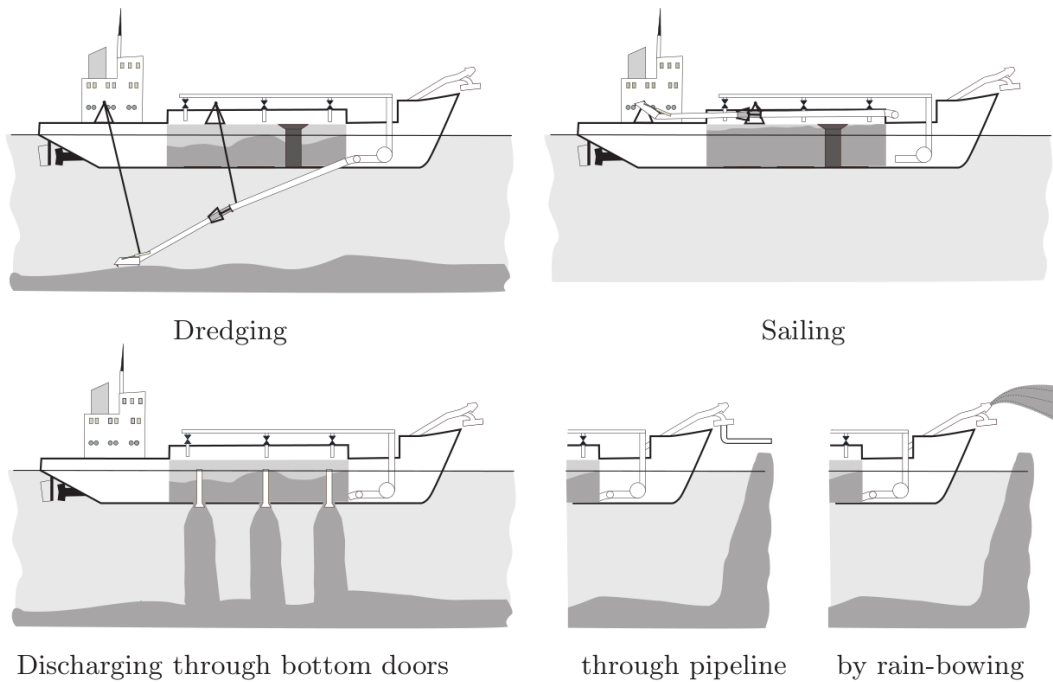


Figure 2.7: The dredge cycle, source: [?]

The bottom doors are able to unload the sand if the water is deep enough. Another option is to pump the sand through pipes to land by using the dredge pump. Before the sand is pumped from the hopper, it needs to be mixed with water using jet pumps. This method costs more time and energy than opening the bottom doors. The dredge pump can also pump the sand through a nozzle overboard, which is called 'rainbowing'. This is done when the water is not deep enough to open the bottom doors, but the TSHD is able to reach the desired discharging area closely enough.

2.2.2 Draghead

Here, the excavation processes in the draghead is explained. A schematic representation of the water and sand flows in the draghead is shown in Figure 2.8.

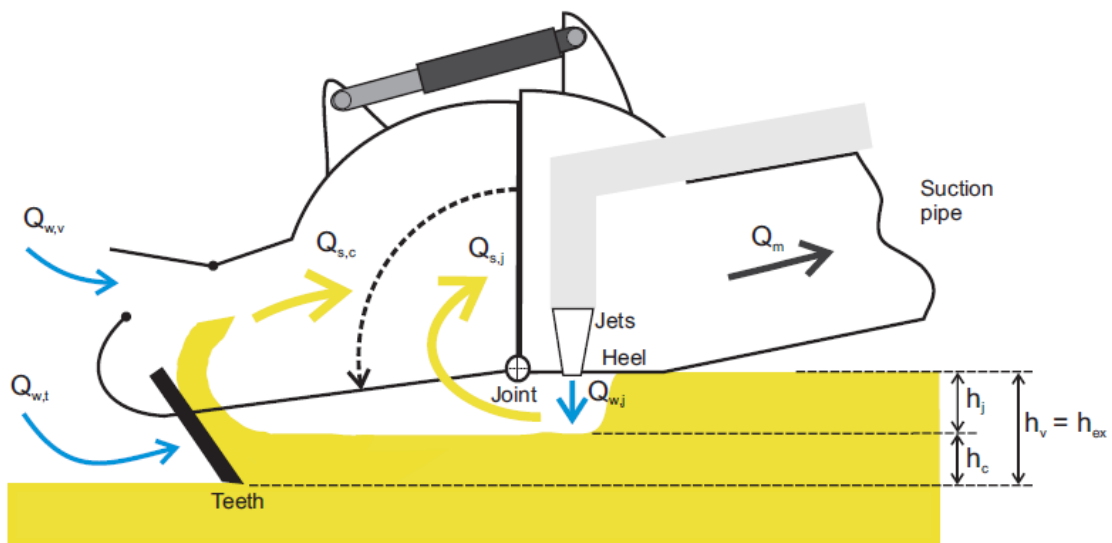


Figure 2.8: A model of the excavation in the draghead, source: [?]

The draghead breaks the coherence of the soil. Sand is excavated both erosive with jets in the heel of the draghead and mechanically with teeth at the back of the draghead. Furthermore, water is sucked up between the teeth and optionally through a valve in the visor of the draghead. With the valve, the density of the mixture can be controlled.

The teeth of the draghead are pulled through the sand, which loosens the soil. With a passive draghead, the visor with teeth is pulled along with the draghead. The visor is mounted at the back of the draghead with a joint. With active dragheads, the visor can be adjusted with a hydraulic cylinder so the depth of the teeth is controlled. Because of the under-pressure in the draghead, created by the dredge pump, loosened soil is carried along with the water. In Figure 2.9 it is visualised how the grains of sand are excavated from a compact sand bed with teeth. Because water is sucked into the sand to fill the increased gaps between the grains, cutting causes a resistance.

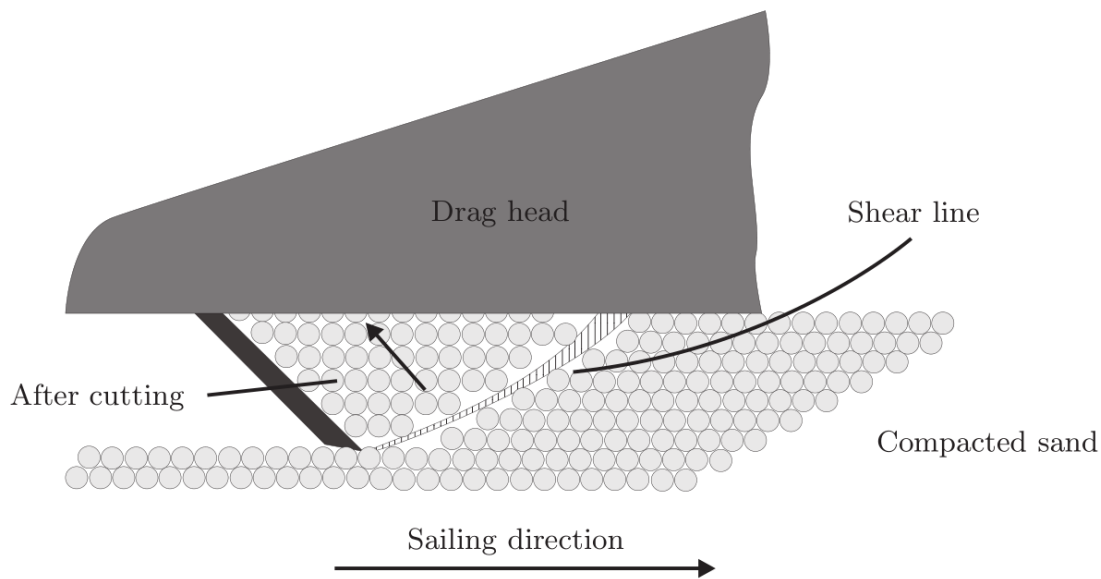


Figure 2.9: Compact and loose sand during cutting, source: [?]

Jets are placed vertically in the heel of the draghead. Jet pumps force water under high pressure into the sand. This way, the underpressure of the pores in the sand while cutting is removed, which lowers the cutting force of the teeth. Also, some sand is made loose enough by the jets so it is sucked up by the flow directly. Applying jets reduce the amount of sand needed to be cut with the teeth. This causes the cutting forces to be reduced as well. From practice it is known that the energy needed for the jet pump is often less than for the propulsion force needed to encounter the cutting force. Therefore, the use of jets often leads to a lower fuel consumption.

The trail force is caused by multiple events. First of all, pulling the teeth through soil causes dilatation of the pore volume of the sand. The resulting sub-pressure increases the grain stresses, which is often the dominant part of the cutting force according to [?]. The cutting force depends on the dimensions of the teeth and the properties of the soil. When the draghead is controlled well, the heel is dragged over the soil, which gives a friction force. When there is a gap between the heel and the soil, the vacuum in the draghead is less which reduces the dredge production. However, when the heel is pulled through the sand, bulldozing occurs which leads to high trail forces. Finally, since the draghead and the suction pipe are pulled through water, drag occurs.

2.3 Trail force and ship motion control

The Dynamic Positioning system (DP-system) of the TSHD controls the motion of the vessel. The trail force disturbs the motion of the TSHD significantly. Therefore, it is important for the system to know the trail force. The DP-system which is currently used by IHC is explained in [?]. It immediately compensates the dredging forces by actuating propellers, rudders and bow thrusters, which improves the tracking performance. The trail force is difficult to measure since force sensors on the suction pipe are vulnerable and need to be changed regularly. Therefore, it is not a robust solution. This is solved for the DP-systems of IHC by estimating the trail force based on another measurement: the pressure difference in draghead. The draghead sucks itself to the bottom which results in a trail force on the draghead. In Figure 2.10, both the measurement of the pressure difference in the draghead and the measured trail force are shown. It is shown that the signals of the trail force and the pressure difference are correlated.

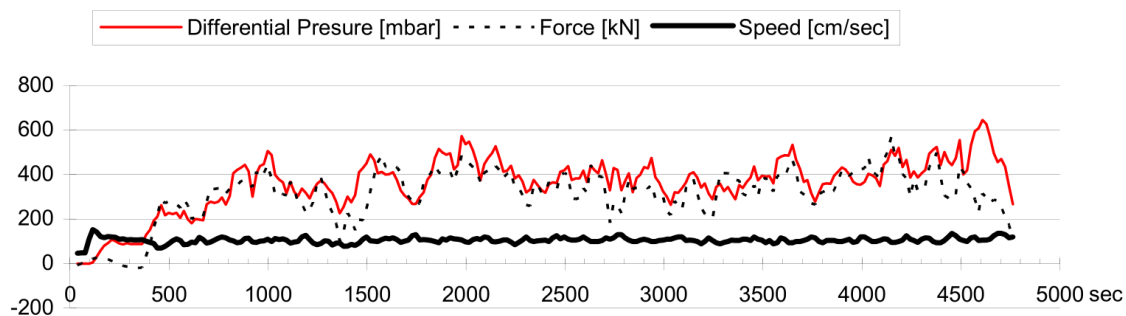


Figure 2.10: Relation between pressure draghead and trail force, source: [?]

By using only the pressure difference measurement, an estimate of the trail force is made. There will be differences between the estimate and the actual force, mainly due to a varying soil type, the use of jet water, pumping speed and sharpness of the draghead teeth. Because of the inaccuracy of the estimation, the velocity of the ship is not controlled optimally. The dredging performance will be improved if the inaccuracy is reduced.

A trail force estimation is also used for feed-forward control in the Trail Speed Controller. This is a basic version of the DP-system. A schematic overview is given in Figure 2.11.

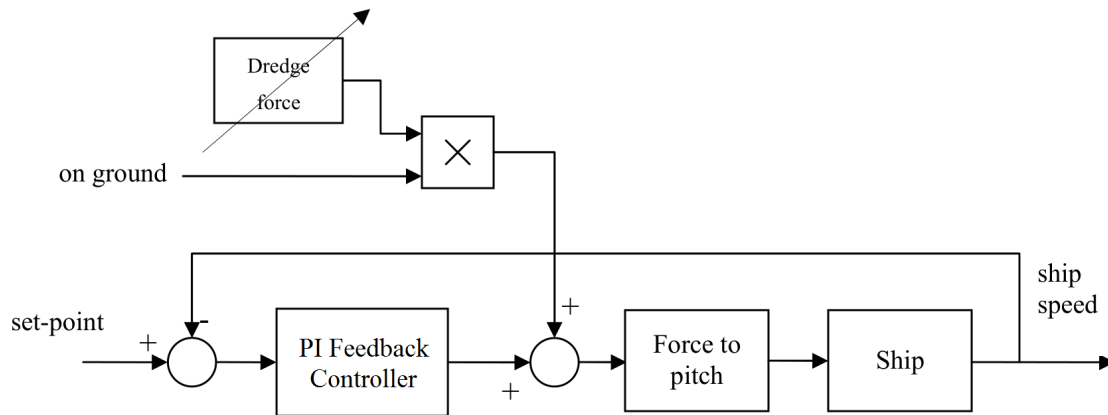


Figure 2.11: Schematic overview of the Trail Speed Controller, source: [?]

The controller ensures the ship keeps the ship speed during dredging at a desired set-point. This is a relatively simple controller, since it only controls the longitudinal speed and only actuates the pitch of the propellers. The Trail Speed Controller uses a combination of feed-forward and feedback control. The velocity is measured and fed back for PI-control to eliminate a steady-state error. An estimation of the trail force is used for feed-forward, which improves the feedback loop since the trail force is directly compensated. A more accurate estimate of the trail force will lead to better control of the velocity.

The DP-systems of IHC work in a similar way, but for all three degrees of freedom of the ship instead of only one. The forces acting on the ship are obtained and used to predict the motion of the ship. The motion is measured as well, using GPS and a compass. If the predicted motion of the ship does not agree with the measured motion, the trail force estimates of both dragheads are slowly adapted. This is done using correction gains on the trail forces. The corrected trail forces are then used to control the propellers and rudders of the ship.

Chapter 3

Modelling the ship dynamics and the trail force

In this chapter, models of the TSHD processes are described in which the trail force and the current are involved. The TSHD will be simulated with these models, so they are desired to be as accurate as possible. Furthermore, a model based estimator will be built to estimate the trail force and the current. The models for the estimator need to be accurate as well, but it is also important to be easily implementable. Therefore, some simplifications are made for these estimator models. The ship dynamics are modelled in Section 3.1. Because the trail force and the current affect the motion of the ship, it is useful to have models available describing the ship motion. The forces in the draghead and the suction pipe are described in Section 3.2 and a model of the trail force is built.

3.1 Ship dynamics

The motion of the ship is observed in a forward (surge) and a sideways (sway) direction. The rotational motion around the vertical axis is also treated, which is called the yaw. Vertical motion and pitch and roll rotations are not taken into account, so only a two dimensional and three degrees of freedom motion is observed. To model the ship dynamics, several input signals are required as shown in Figure 3.1.

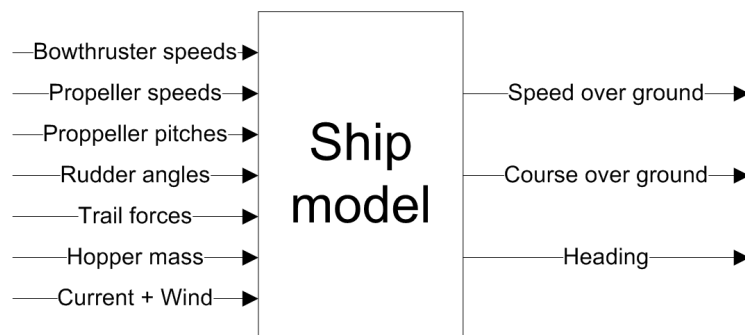


Figure 3.1: Input and output signals of the modelled ship dynamics

As shown in Figure 3.2, the following forces which affect the motion of the ship are considered:

- Drag force from the current and wind
- Trail force from the dragheads
- Thrust force from propellers and rudders
- Thrust force from bow thrusters

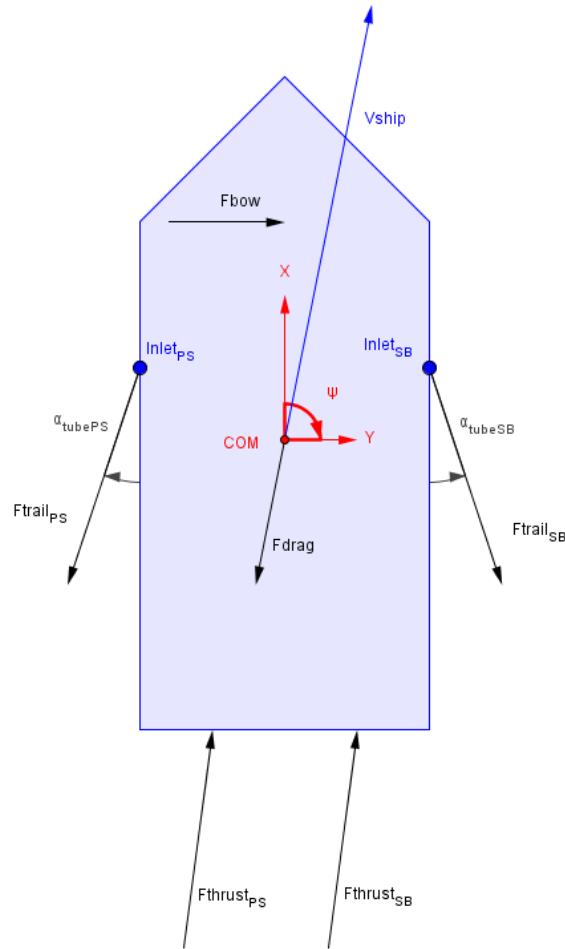


Figure 3.2: Forces on the modelled ship and the coordinate system

In this section, the forces are modelled so the the motion of the ship can be determined. The forces are obtained in the same directions as the motion is observed: forward (x), sideways (y, starbord positive) and rotational (ψ , clockwise positive). For the simulation model, these forces are required to be as accurate as possible. When possible, they will be validated using measurement data from the sea trial of the TSHD 'Jun Yang 1'. For the estimator model, the forces are sometimes simplified and lookup tables are approximated with equations so the tables do not need to be included into the estimator. The following signals of the ship are needed:

Table 3.1: Input signals for the ship model. Most signals arise from both sides of the TSHD and are therefore double.

input	description
$F_{tr.mod}$	modelled trail force (2x)
α_{tube}	horizontal tube angle (2x)
ϕ	propeller pitch (2x)
α_{rud}	rudder angle (2x)
ω_{prop}	propeller speed (2x)
ω_{bow}	bow thrusters speed
m	ship mass
v_c, ψ_c	current speed and angle

3.1.1 Accelerations

The forward, sideways and rotational accelerations of the ship are obtained to be able to model the motion of the ship. This is done using the mass matrix and the force vector, which contains the resultant forces on the ship.

$$\frac{d}{dt} \begin{bmatrix} v_x \\ v_y \\ \psi \end{bmatrix} = M^{-1} \begin{bmatrix} F_{tot.x} \\ F_{tot.y} \\ M_{tot.\psi} \end{bmatrix} \quad (3.1)$$

The mass matrix contains the mass and rotational inertia of the ship including the mass of the hopper. The inertia is approximated using the assumption that the ship is a block with a uniform density: $I = \frac{1}{12}m(L^2 + B^2)$. Furthermore, the added mass of the water a is included. This is needed because the ship movement causes movement of water around the ship. Therefore, added mass increases the mass and inertia of the ship and depends on the draft of the ship. The cross terms $a_{y\psi}$ represent the added mass in sway direction due to a unit yaw acceleration, and also the added mass in yaw direction due to a unit sway acceleration. These cross terms are not negligible and therefore included.

$$M = \begin{bmatrix} m_{ship} + a_{xx} & 0 & 0 \\ 0 & m_{ship} + a_{yy} & a_{y\psi} \\ 0 & a_{y\psi} & I_{ship} + a_{\psi\psi} \end{bmatrix} \quad (3.2)$$

The accelerations are integrated to obtain the velocities of the ship in forward, sideways and rotational direction. The rotational velocity (or heading rate) is integrated again to obtain the heading. The relative velocity of the ship through water is required to obtain drag and thrust. Therefore, the velocity of the current v_c and direction ψ_c is needed to correct the speed over ground to the relative speed through water.

$$v_{xr} = v_x - v_c \cos(\psi_c - \psi) \quad (3.3)$$

$$v_{yr} = v_y - v_c \sin(\psi_c - \psi) \quad (3.4)$$

3.1.2 Propeller

The propulsion of the ship is performed by the two propellers at the stern. Their thrust is controlled by adapting the pitch angle of the blades. This is explained in Section 2.1.

Simulation model

Tables with thrust forces and corresponding pitch values are available for the Jun Yang 1. These values are obtained given the ship speed, propeller speed and used propulsion power. The tables are based on empirical relations which are fitted on data from model tests. The tables are defined at the complete range of states where the thrust force, propeller speed, pitch ratio and ship speed are located during dredging. However, since the simulation model had problems to obtain the thrust based on a given pitch with these tables, an equation is used. By fitting an equation on the table values, an accurate model is found for the complete range of states. The propulsion force of each propeller is modelled by Equation 3.5. This is based on the idea that the thrust force is caused by the slip, which is the difference between the forward propeller speed and the ship speed.

$$F_{prop} = c_1 |\omega| \cdot |\phi|^{c_2} \cdot (c_3 \cdot \omega \cdot \phi - v_{xr}) \quad (3.5)$$

The thrust force [kN] depends on the propeller speed ω [rpm], the pitch ratio ϕ [-] and the forward velocity of the ship through water v_{xr} [kn]. The pitch ratio equals the pitch divided by the diameter of the propeller. The coefficients c_1 , c_2 and c_3 are fitted on thrust force tables using least squares optimization. For the Jun Yang 1, the coefficients are found to be:

$$c = [0.5315 \quad 0.1312 \quad 0.1535] \quad (3.6)$$

Validation

The model of the thrust force has a root mean square error of 51.2 kN compared to the values from the tables. Especially around the dredging velocity, the error between the trail force model and the table values is acceptable.

The thrust force model is compared to a measurement of the thrust force as well, which uses axially placed strain gauges on the propeller shafts. The measurement of the force is unfortunately not reliable because the signal contains an offset and spikes. Furthermore, the signal is often dead. However, it is still possible to compare the model with the measurement.

To be able to validate, a time period is needed when the ship sails with dredging speed, which is about 1 m/s. This is the state where the model needs to be accurate. The current of the water is required to be known so the relative velocity is obtained. Measurement data of June 22 10:30 - 12:40 is found where:

- the ship speed is low: around 1 m/s
- the current is estimated in real time by the DP-system
- a thrust measurement is available, however this contains noise and an offset

The offsets on the pitch and thrust measurements are removed so Equation 3.5 can be used to obtain the modelled thrust force of both propellers. They are compared with the measurements in Figure 3.3. It shows that the error between the modelled thrust force and the measurements is small. To quantify the performance of the model, the Variance Accounted For [?] and the Root Mean Square Error are obtained for both propellers, see Table 3.2.

Table 3.2: Performance of the modelled trust force, calculated for data between 11:00 and 12:40

Propeller:	VAF:	RMSE:
Port side	98.4 %	52 kN
Starboard side	86.0 %	118 kN

These values are obtained for the time period 11:00 - 12:40 to exclude the peaks at 10:33 and 10:58. It is clear that the peaks in the measurement of the starboard propeller lead to a lower VAF and a higher RMSE, but from visual inspection it can be concluded that the model fits well for the purpose. When applying Equation 3.5 on other periods of the measurement data, the relative speed through water is not known and the speed over ground has to be used. The thrust force model is still able to deliver an approximation, but a higher offset is often observed. It is assumed that this is mainly because of the current, so Equation 3.5 is considered to be a useful model.

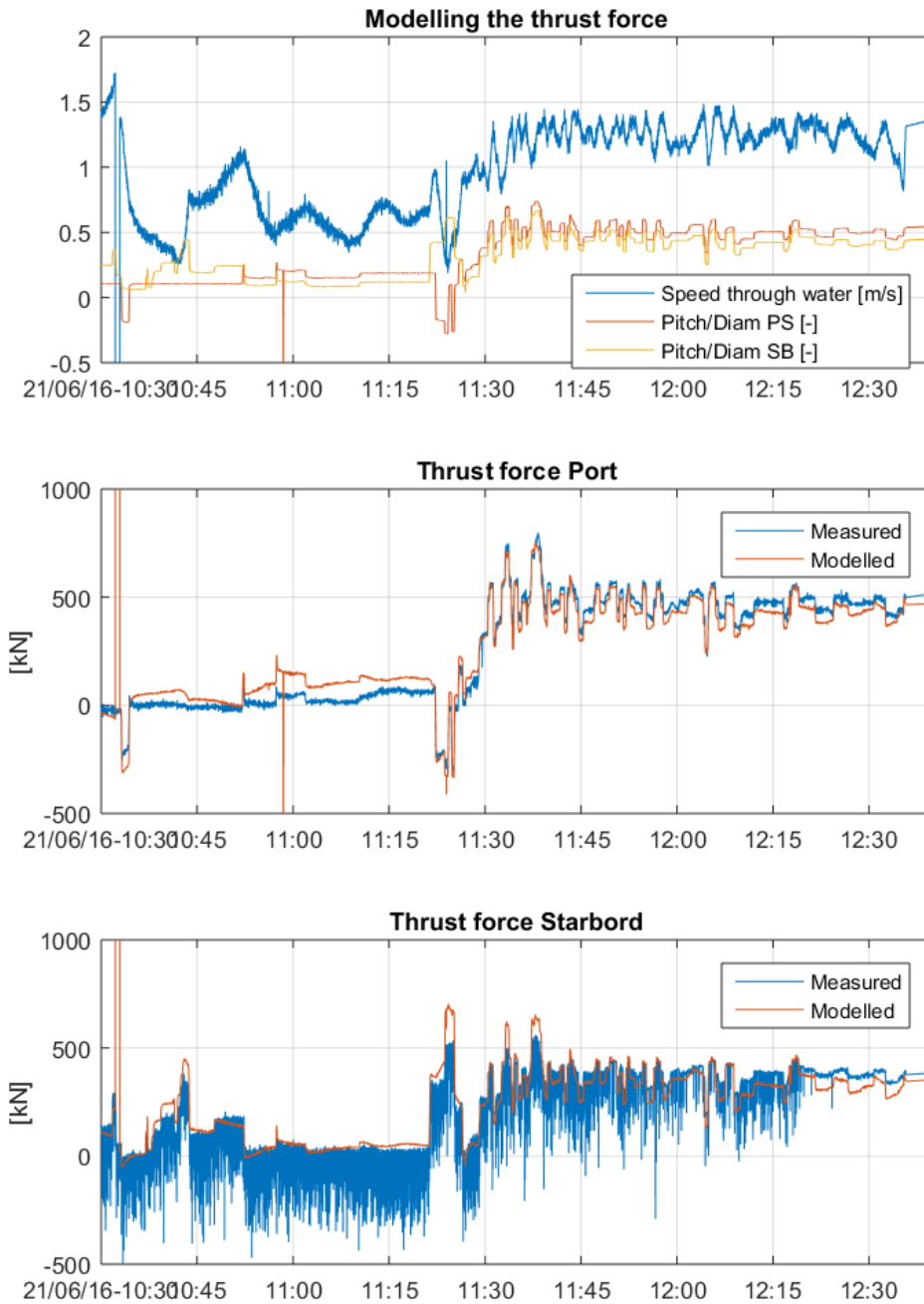


Figure 3.3: Validation of the modelled thrust force using measurements. Note that the frequent peaks in the starboard measurement are pointing downwards and might give a distorted view of the real values, which are at the top.

Estimator model

The propeller speed, relative ship speed and pitch ratio are all available for the estimator, so the estimator will also use Equation 3.5.

3.1.3 Rudder

By turning the rudders sideways force is created on the rudders. This results in a moment which turns the ship.

Simulation model

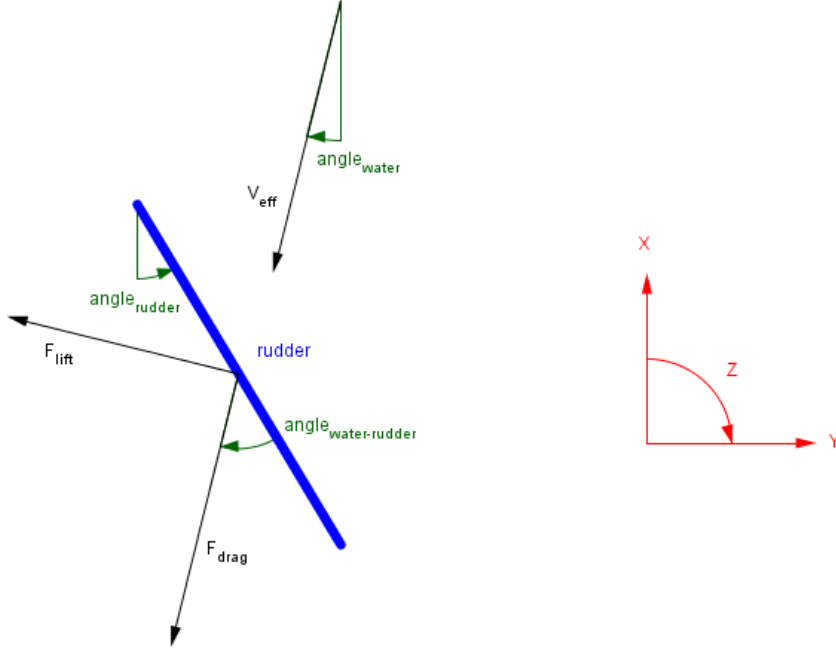


Figure 3.4: Angles and forces of the flow on a rudder

The force acting on each rudder is represented by the drag force and lift force which are parallel and perpendicular on the water velocity respectively, as shown in Figure 3.4. They are modelled with the following equations:

$$\begin{bmatrix} F_{drag} \\ F_{lift} \end{bmatrix} = \begin{bmatrix} C_{drag} \\ C_{lift} \end{bmatrix} \frac{1}{2} \rho_w \cdot V_{eff}^2 \quad (3.7)$$

The angle of the current on the rudder is obtained by adding the angle of the effective current and the angle of the rudder. This angle is used to lookup the drag and lift coefficients of the rudder C_{drag} and C_{lift} from a table, which already includes the rudder area. A table is created for the Jun Yang 1, based on empirical relations which are fitted on data from model tests. The force of each propeller as described in Section 3.1.2 and their associated rudder have the following resulting forward and sideways forces on the ship:

$$F_{thrust.x} = F_{prop} - F_{drag} \cos(\alpha_{water}) + F_{lift} \sin(\alpha_{water}) \quad (3.8)$$

$$F_{thrust.y} = -F_{drag} \sin(\alpha_{water}) - F_{lift} \cos(\alpha_{water}) \quad (3.9)$$

Since the rudders are placed at y_{rud} from the centreline and x_{rud} behind the center of mass of the ship, the forces result in a moment on the ship:

$$M_{thrust} = y_{rud}(F_{thrust.x.PS} - F_{thrust.x.SB}) - x_{rud}(F_{thrust.y.PS} + F_{thrust.y.SB}) \quad (3.10)$$

The effective velocity of the current on the rudder is not equal to the velocity of the ship through water as shown below.

$$V_{rud.x} = \sqrt{V_{ship.x}(1-w) + C_T F_{prop}} \quad (3.11)$$

$$V_{rud.y} = V_{ship.y} - \dot{\psi} L_{rud-cog} \quad (3.12)$$

This is because the rudder is placed at the back of the ship. Therefore, the relative velocity is reduced with a factor w because of the hull friction of the ship as explained in [?]. The velocity is then increased by the thrust force of the propellers as explained by [?]. The factor $C_T \approx \frac{6.4}{\pi \rho h D_p}$ depends on the height of the rudder h and the diameter of the propeller D_p .

Estimator model

For the estimator, some simplifications are made so no lookup tables are required. The following expressions for drag and lift coefficients approximate the values from the tables.

$$C_{drag} = 1.6 \cdot \sin(\alpha_{rud})^2 \quad (3.13)$$

$$C_{lift} = 1.5 \cdot \sin(2 \cdot \alpha_{rud}) \quad (3.14)$$

Furthermore, the velocity of the ship has little effect on the velocity of the flow on the rudder. The current on the rudder is practically only caused by the propellers, especially during dredging because of the high thrust force and low ship velocity. This assumption enables the following simplification of the effective velocity on the rudder, which is considered to be parallel on the ship:

$$V_{eff}^2 = C_T F_{prop} \quad (3.15)$$

So the resulting forces of each propeller and rudder on the ship are:

$$F_{thrust.x} = F_{prop} - 1.6 \cdot \sin(\alpha_{rud})^2 \cdot \frac{1}{2} \rho_w \cdot C_T \cdot F_{prop} \quad (3.16)$$

$$F_{thrust.y} = 1.5 \cdot \sin(2 \cdot \alpha_{rud}) \cdot \frac{1}{2} \rho_w \cdot C_T \cdot F_{prop} \quad (3.17)$$

These forces result in the moment as given in Equation 3.10.

3.1.4 Drag force

The water flow on the hull of the ship causes a drag force on the ship which needs to be modelled. Since we focus on the processes during dredging, the forces need to be representable around 1 m/s. At this low velocity, the drag force is assumed to be quadratically related to the velocity through water v_r . The wind causes a resistance as well and is modelled in a similar way.

Simulation model

The drag affects the ship in the three motion directions so the three components of the force are obtained:

$$F_{drag.x} = -v_r |v_r| \cdot c_{d.x} \quad (3.18)$$

$$F_{drag.y} = -v_r |v_r| \cdot c_{d.y} \quad (3.19)$$

$$M_{drag} = -v_r |v_r| \cdot c_{d.rot} - \dot{\psi} |\dot{\psi}| \cdot c_{d.\psi} \quad (3.20)$$

With the drag coefficients c_d in three motion directions depending on the direction of the current on the ship, the draft of the ship and the waterdepth. Since the weight of the ship increases during dredging, the draft and therefore the drag force increases as well. The drag coefficients are interpolated from values in lookup tables. These are based on empirical relations which are fitted on data from model tests. They already include the density of the water and the area's of the ship.

$$c_{d.\psi} = c_{d.y} \cdot L_{sh}^3 / 32 \quad (3.21)$$

The drag resulting from a rotational velocity is mainly caused by the sideways drag. The sideways drag is assumed to be uniform along the length of the ship and used to obtain the rotational drag coefficients.

Validation

To validate the model, measurement data is required with a situation where:

- a correct thrust force measurement signal is available
- a correct relative velocity signal is available
- the ship is at dredging velocity: $v \approx 1$ m/s
- the ship is not dredging, so the assumption $F_{thrust} = F_{drag}$ is valid
- the rudders are straight
- the bow thrusters are off
- there is no or little relative sideways velocity

At June 21th 10:44 - 10:47 some measurement data is found satisfying these requirements. These conditions are not met all together very often since the ship is mostly either sailing at high speed or dredging at low speed, but not sailing at low speed. Besides that, the relative velocity and thrust force signals are frequently dead.

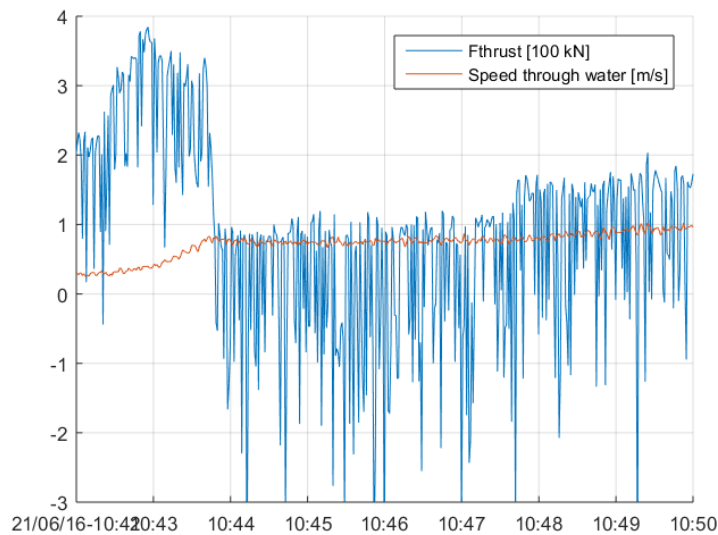


Figure 3.5: Measured thrust force at constant velocity to validate the drag force

During the three minutes between 10:44 - 10:47, the relative velocity is 0.8 m/s and the thrust force is around 90 kN - 100 kN, as shown in Figure 3.5. The ship's mass is 0.7 times the mass of a full ship, so the drag force should be around 50 kN according to the table and the corresponding equations. However, the drag is two times as much than expected. This is probably because the tubes are almost lowered to the bottom, which causes additional drag. Another reason could be that the velocity or thrust signal is not accurate. The relative velocity is obtained by using a current estimate, which could be different than the actual current. Furthermore, the thrust force measurement is not very reliable and hard to read because of the spikes. If better measurements are available, the drag coefficients could be determined more accurately. Since the trail force is up to 10 times higher than the drag force during dredging, the impact of an eventual mismatch is limited. Therefore, equations 3.18-3.20 are used for the simulation model.

Estimator model

For the estimator, the equations are simplified so no lookup table is needed. It is possible to implement the drag tables in the estimator but it saves effort and complexity by setting up equations as an alternative. It is expected that the equations will not differ much from the values from the tables.

$$F_{drag.x} = -v_r |v_r| \cdot (c_{x.min} + \frac{c_{x.max} - c_{x.min}}{m_{sf} - m_{se}} (m - m_{se})) \quad (3.22)$$

$$F_{drag.y} = -v_r |v_r| \cdot (c_{y.min} + \frac{c_{y.max} - c_{y.min}}{m_{sf} - m_{se}} (m - m_{se})) \quad (3.23)$$

$$M_{drag} = -\dot{\psi} |\dot{\psi}| \cdot (c_{y.min} + \frac{c_{y.max} - c_{y.min}}{m_{sf} - m_{se}} (m - m_{se})) \cdot L_{sh}^3 / 32 \quad (3.24)$$

The velocity of the ship through water in forward, sideways and rotational direction is used for the drag in the corresponding directions. The effect of the changing draft, is taken into account by including the mass of the ship into the equations. The forward and sideways drag coefficients are obtained for both an empty and a full ship so they can be interpolated for all ship masses. For forward drag, the drag increases from $c_{x.min} = 15 \text{ kN}/(\text{m/s})^2$ to $c_{x.max} = 130 \text{ kN}/(\text{m/s})^2$. For sideways drag, the drag increases from $c_{y.min} = 300 \text{ kN}/(\text{m/s})^2$ to $c_{y.max} = 1500 \text{ kN}/(\text{m/s})^2$. The drag coefficients are adopted from the tables. The rotational drag is assumed to be only caused by the rotational velocity and therefore determined using Equation 3.21 as well. Since there is no measurement data available of the wind and the wind fluctuates too much to estimate this accurately, the wind is neglected in the estimator.

3.1.5 Pipe forces

The trail force acting on the draghead causes a large disturbance on the motion of the ship. The magnitude of the trail force in the draghead is modelled in Section 3.2. The suction pipes are mounted on the inlets at the side of the ship. The angle between the pipe and the ship are denoted with α_{tube} , where a positive angle represents outward pointing pipes. The trail force does not only affect the forward motion, but also the sideways and rotational motion. The inlets are located at x_{inlet} ahead and y_{inlet} beside the centre of mass of the ship.

Simulation model

The resulting forces on the motion of the ship from the trail forces is obtained as:

$$F_{tr.x} = -\cos(\alpha_{tube.sb}) \cdot F_{tr.sb} - \cos(\alpha_{tube.ps}) \cdot F_{tr.ps} \quad (3.25)$$

$$F_{tr.y} = \sin(\alpha_{tube.sb}) \cdot F_{tr.sb} - \sin(\alpha_{tube.ps}) \cdot F_{tr.ps} \quad (3.26)$$

$$M_{tr} = y_{inlet} \cdot (\cos(\alpha_{tube.sb}) \cdot F_{tr.sb} - \cos(\alpha_{tube.ps}) \cdot F_{tr.ps}) + x_{inlet} \cdot F_{tr.y} \quad (3.27)$$

The angle of the suction pipe changes with the movement of the ship. Since the sideways forces and motion of the draghead and suction pipe are small, it is assumed that the draghead is only dragged in the direction of the pipe. The velocity of the inlets where the pipes are mounted on the ship are obtained in x and y direction. They depend on the rotational velocity of the ship $\dot{\psi}$ as well.

$$v_{x.SBinlet} = v_{x.ship} - y_{inlet} \cdot \dot{\psi} \quad (3.28)$$

$$v_{y.SBinlet} = v_{y.ship} + x_{inlet} \cdot \dot{\psi} \quad (3.29)$$

$$v_{x.PSinlet} = v_{x.ship} + y_{inlet} \cdot \dot{\psi} \quad (3.30)$$

$$v_{y.PSinlet} = v_{y.ship} + x_{inlet} \cdot \dot{\psi} \quad (3.31)$$

The inlet velocities are used to determine the rate of change of the pipe angles. The angles change with the motion of the ship.

$$\dot{\alpha}_{SB} = \frac{1}{L_{pipe}}(-v_{x.SBinlet} \sin(\alpha_{SB}) - v_{y.SBinlet} \cos(\alpha_{SB})) + \dot{\psi} \quad (3.32)$$

$$\dot{\alpha}_{PS} = \frac{1}{L_{pipe}}(-v_{x.PSinlet} \sin(\alpha_{PS}) + v_{y.PSinlet} \cos(\alpha_{PS})) - \dot{\psi} \quad (3.33)$$

To determine the velocity of the dragheads in the direction of the pipe, the velocity of the inlets and the angle of the pipes are needed as well.

$$v_{dh.SB} = v_{x.SBinlet} \cos(\alpha_{SB}) - v_{y.SBinlet} \sin(\alpha_{SB}) \quad (3.34)$$

$$v_{dh.PS} = v_{x.PSinlet} \cos(\alpha_{PS}) + v_{y.PSinlet} \sin(\alpha_{PS}) \quad (3.35)$$

Validation

Because all equations are geometrically determined, these models are accurate.

Estimator model

The trail force of the dragheads will be modelled in Section 3.2. The effect of the trail force of the draghead on the motion of the ship is determined using Equations 3.25-3.27.

3.1.6 Bow thrusters

The propellers of the bow thrusters are driven by electro motors. Their rotational velocity is measured and is used to determine the delivered thrust. The thrust increases quadratically with the speed. The effective thrust that the bow thrusters have on the ship depends on the velocity of the ship as well. At standstill, the thrusters have maximal effect. However, the efficiency reduces with an increasing speed, so this effect will be included. From experience we know that the effective thrust reduces to less than half at a velocity of two knots and to almost zero at velocities above five knots. This is included in the expression of the thrust of a bow thruster as follows:

$$F_{bow} = F_{max} \cdot \left(\frac{\omega}{\omega_{max}}\right)^2 \cdot \max(0, (1 - \frac{|v|}{5}))^{1.4} \quad (3.36)$$

With the velocity v translated to knots, and the maximum thrust of the JunYang 1 $F_{max} = 78$ kN at $\omega_{max} = 323$ rpm for each of the two bow thrusters. They are placed x_{bow} ahead of the center of mass and they have the following resultant forces on the ship:

$$F_{bow.x} = 0 \quad (3.37)$$

$$F_{bow.y} = F_{bow} \quad (3.38)$$

$$M_{bow} = x_{bow} \cdot F_{bow} \quad (3.39)$$

3.1.7 Conclusion

In this section, the ship dynamics are modelled. By obtaining all forces in the direction of all three degrees of freedom of the ship, the motion of the ship is modelled. The modelled ship motion is used in both the simulation model and the estimator model, but their properties are different. Several tables, based on empirical relations and ship characteristics, are used to model the forces on the ship. These tables are used for the simulation model when possible, so the accuracy is ensured and the simulated results will be realistic. The estimator model uses approximations with equations since implementing the estimator will then be less complex. Furthermore, the models are nonlinear and not always fully accurate, especially the drag force. This has to be taken into account when working with these models.

3.2 Trail force

In this section, the forces in the draghead and the suction pipe are described. A model of the trail force is built which requires the inputs as shown in Figure 3.6.

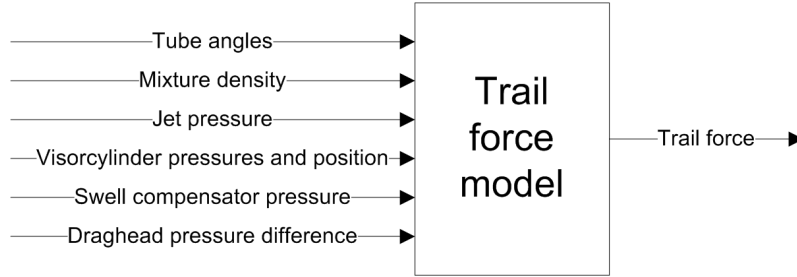


Figure 3.6: Inputs and output of the trail force model

The trail force is caused by the interaction between the bottom and the draghead. In this section, the forces on the teeth and the heel are modelled as shown in Figure 3.7 by observing the moments around the visor joint and the cardan joint. The trail force is then obtained by adding the horizontal components of the forces in the teeth and heel:

$$\hat{F}_{trail} = F_{cut.h} + F_{heel.h} \quad (3.40)$$

The motion of the TSHD is observed in the horizontal plane and therefore, we are interested in the horizontal component of the trail force.

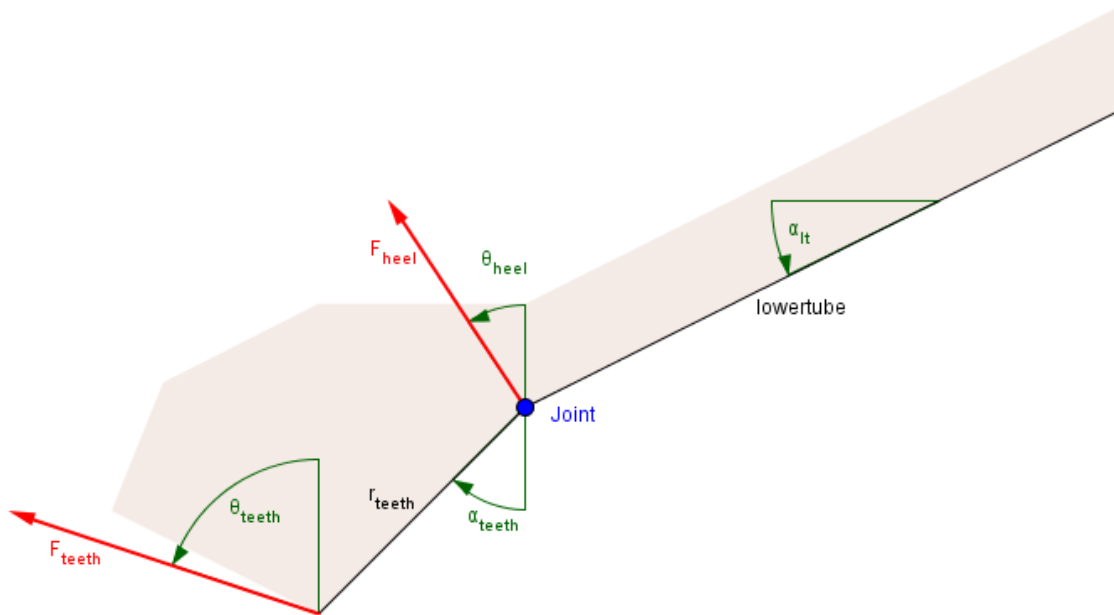


Figure 3.7: The forces on the heel and the blade

This method of trail force modelling requires the following steps:

1. The cutting force is obtained by assuming the visor is in an equilibrium. The visor cylinders, the visor's weight, the pressure difference in the draghead and the force of the soil on the teeth affect the rotation of the visor around the joint. By modelling all influences and assuming $\sum M = 0$, the moment of the teeth around the visor joint is obtained. Using the angle of

the teeth and the cutting theory of Miedema [?], the horizontal and vertical components of the cutting force are approximated.

2. The friction force in the heel is obtained by assuming the lower suction tube is in an equilibrium. The gravity, swell compensator, jets, differential pressure, cutting force and heel force exert a moment on the lower suction tube around the cardan joint. Using the assumption $\sum M = 0$ and the in (1) obtained cutting force, the moment of the heel friction at the cardan joint is obtained.
3. The cutting force and the friction force in the heel give the trail force. The horizontal components of the cutting and heel forces are added up.

The following measurements of the suction pipe and the draghead are needed:

Table 3.3: Input signals for the trail force model

symbol	description
α_{lt}	vertical angle of the lower tube
α_{ut}	vertical angle of the upper tube
ρ_{mix}	density of the sand/water mixture in the pipe
p_{jet}	output pressure of the last jetpump
p_{sc}	pressure in the swell compensator
$p_{vc.rod}$	pressure in the rod side of the visor cylinders
$p_{vc.bot}$	pressure in the bottom side of the visor cylinders
Δp	pressure difference in the draghead
x_{vc}	position of the visor cylinders

3.2.1 Visor

The visor is mounted on the draghead and is able to rotate around the visor's joint. See Figure 3.8 for a technical illustration of the complete draghead. The teeth are mounted at the bottom side of the visor. The JunYang 1 is equipped with 'Wild Dragon' dragheads. These use two rows of teeth with integrated jets, which excavate sand with lower cutting forces than conventional ones. The visor cylinders are used to control the position of the visor and thereby the cutting depth.

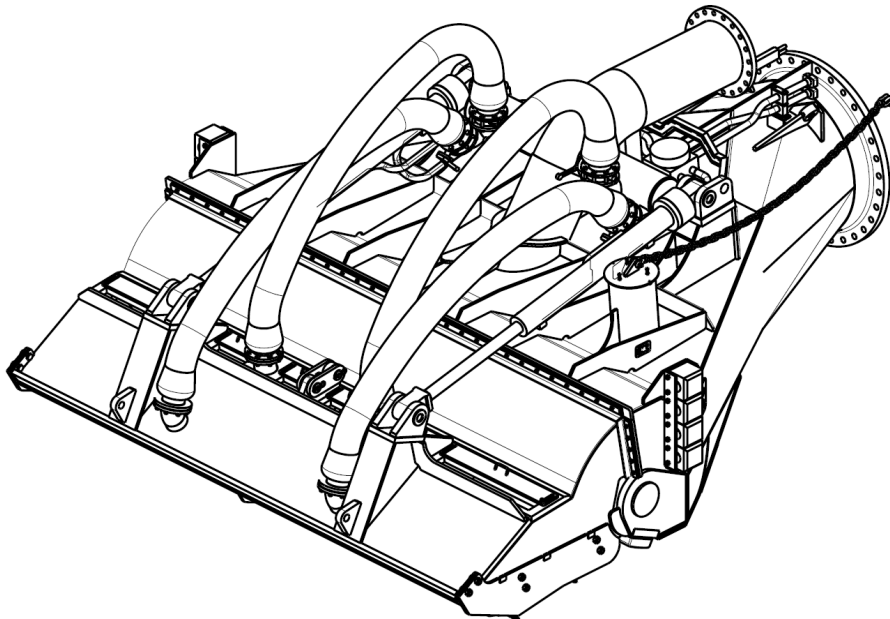


Figure 3.8: Technical illustration of the draghead, source: IHC

The following forces affect the angle of the visor around the joint:

- Force of the visor cylinders
- Force resulting from the pressure difference in the visor
- Gravitational force
- Cutting force

The cutting force is not directly measured, but it is possible to obtain by deriving the other three forces using measurements. Therefore, the geometry of the visor is used, which is shown in Figure 3.9:

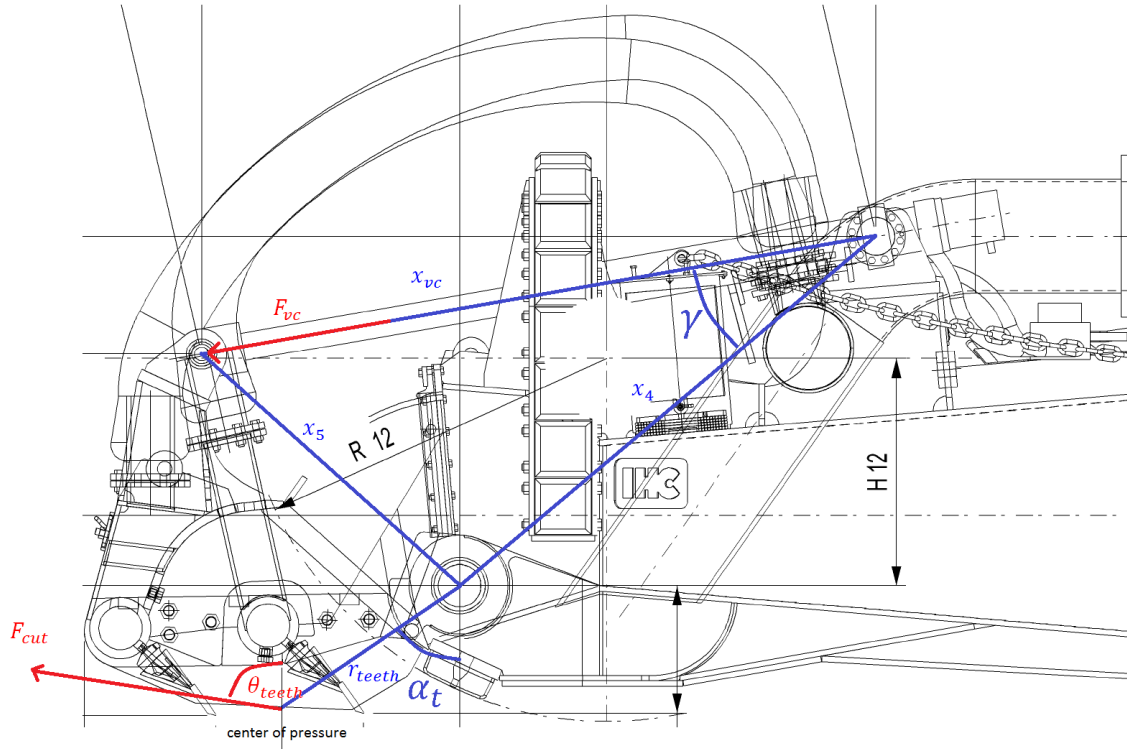


Figure 3.9: Geometry of the visor, source: IHC

The visor's cylinders hold the visor at the desired position and push the visor downwards to counteract for the cutting force. The pressure of both sides of the visor's cylinder is measured, as well as the position. The position is used to determine the distance of the force perpendicular on the joint.

$$M_{vc} = F_{vc} \cdot x_4 \cdot \sin(\gamma) \quad (3.41)$$

$$F_{vc} = A_{bot} p_{vc.bot} - A_{rod} p_{vc.rod} \quad (3.42)$$

$$\gamma = \cos^{-1} \left(\frac{x_4^2 + x_{vc}^2 - x_5^2}{2 \cdot x_4 \cdot x_{vc}} \right) \quad (3.43)$$

The pressure difference in the draghead created by the dredgepump results in a moment on the visor as well. The opening at the bottom of the visor pulls the visor downwards. It has the same width as the draghead w_{dh} , a length of L_{bot} and the center of this area is located at R_{bot} from the joint. The pressure difference in the cross section of the visor shoving into the draghead pulls the visor upwards. This opening is w_{dh} wide as well, has a length of L_{top} and its center is located at R_{top} from the joint.

$$M_{\Delta p} = \Delta p \cdot w_{dh} \cdot (L_{bot} R_{bot} - L_{top} R_{top}) \quad (3.44)$$

Finally, the gravity creates a moment on the visor. The weight of the visor can be represented by a point mass at a certain distance R from the joint.

$$M_g = gW_{visor}R \quad (3.45)$$

The three moments around the joint are shown in Figure 3.10 during a dredging cycle. It can be seen that the moment resulting from the visor cylinders fluctuates and contains a lot of peaks.

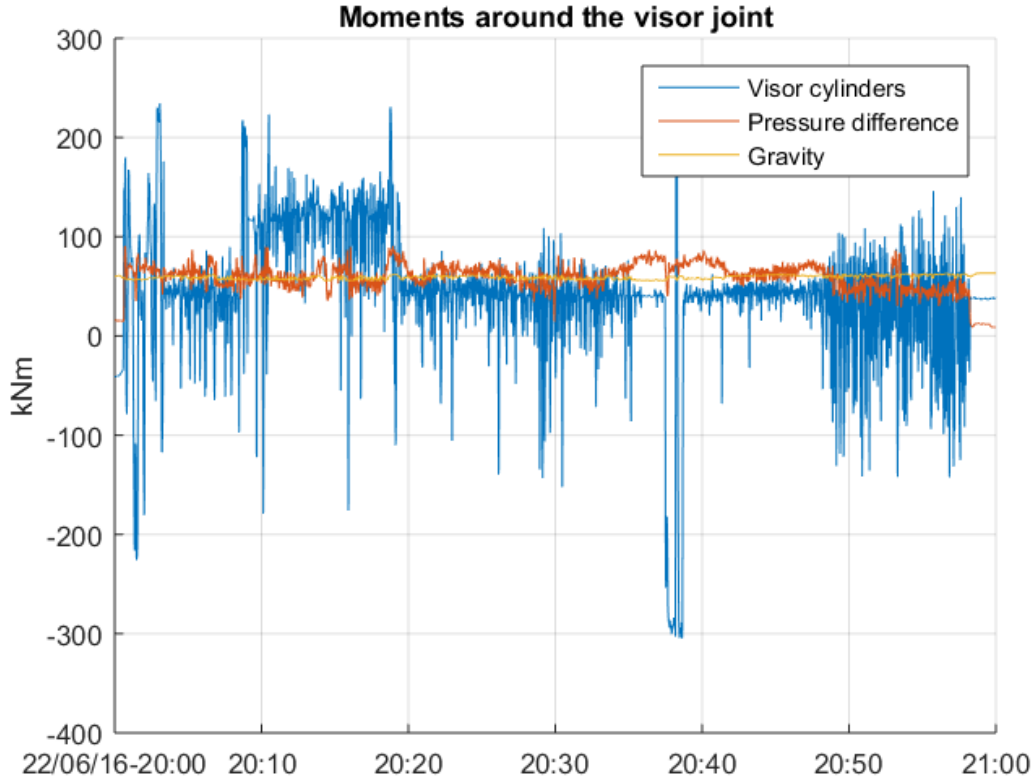


Figure 3.10: Moments around the visor joint during dredging

Using the assumption of a static equilibrium, so $\sum M = 0$, the remaining moment around the joint is assigned to the cutting force on the blade. This simplification is made since we are only interested in the slow dynamics.

$$M_{cut} = M_{vc} + M_{\Delta p} + M_g \quad (3.46)$$

$$F_{cut} = \frac{M_{cut}}{r_{teeth} \sin(\alpha_{teeth} + \theta_{teeth})} \quad (3.47)$$

$$F_{cut.h} = F_{cut} \sin(\theta_{teeth}) \quad (3.48)$$

The angle of the cutting force θ_{teeth} is not known, but it can be estimated using Miedema's cutting theory. This is explained in Appendix C. To make the estimate, it is needed to determine whether cavitation cutting takes place. This is often the case during dredging with the usual conditions (dredging depth, velocity, layer height, sand properties) so cavitation cutting is assumed. Therefore, the following angle of the cutting force is used:

$$\theta_{teeth} = 90^\circ - \arctan\left(\frac{45 - \alpha_b}{75}\right) \quad (3.49)$$

Where α_b is the angle of the blade. For small blade angles, the friction angle will be over 90 degrees, since the blade is then pulled downwards by the soil.

3.2.2 Lower tube

The lower tube is connected to the upper tube with the cardan joint. It is able to rotate around the joint. The TSHD 'Jun Ynag 1' can be equipped with different lengths of suction tubes, depending on the dredging depth. The maximum dredging depth is 40 meter, 60 meter as shown in Figure 3.11, or even 90 meter (only one draghead). The suction tube observed here has a length of 57 meter and has a maximum dredging depth of 40 meter. The lower tube has a diameter of 1.2 meter and weighs about 45 tons.

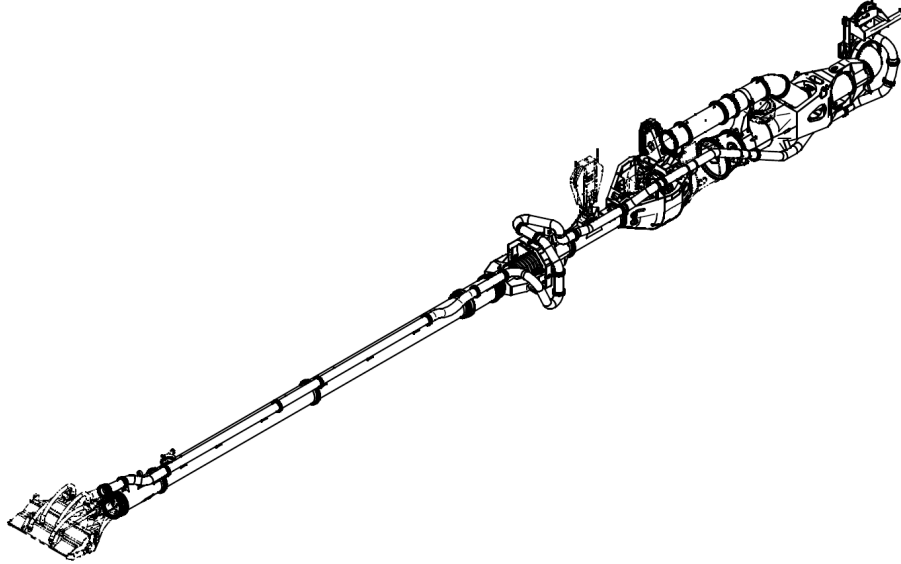


Figure 3.11: Technical illustration of the suction tube, source: IHC

The following forces affect the angle of the lower tube around the cardan joint, as illustrated in Figure 3.12 :

- Force in the swell compensator's cable
- Force resulting from the pressure difference in the visor
- Gravitational force
- Impulse force of the jet water
- Cutting force
- Friction force of the soil on the heel

The friction force in the heel is not measured, but can be determined by obtaining the other influences. The first 4 can be determined using measurements and the cutting force is determined in the previous part. The forces are observed as shown in the figure below. The unknown forces in the heel are the ground force, which is vertical, and the friction force, which is horizontal.

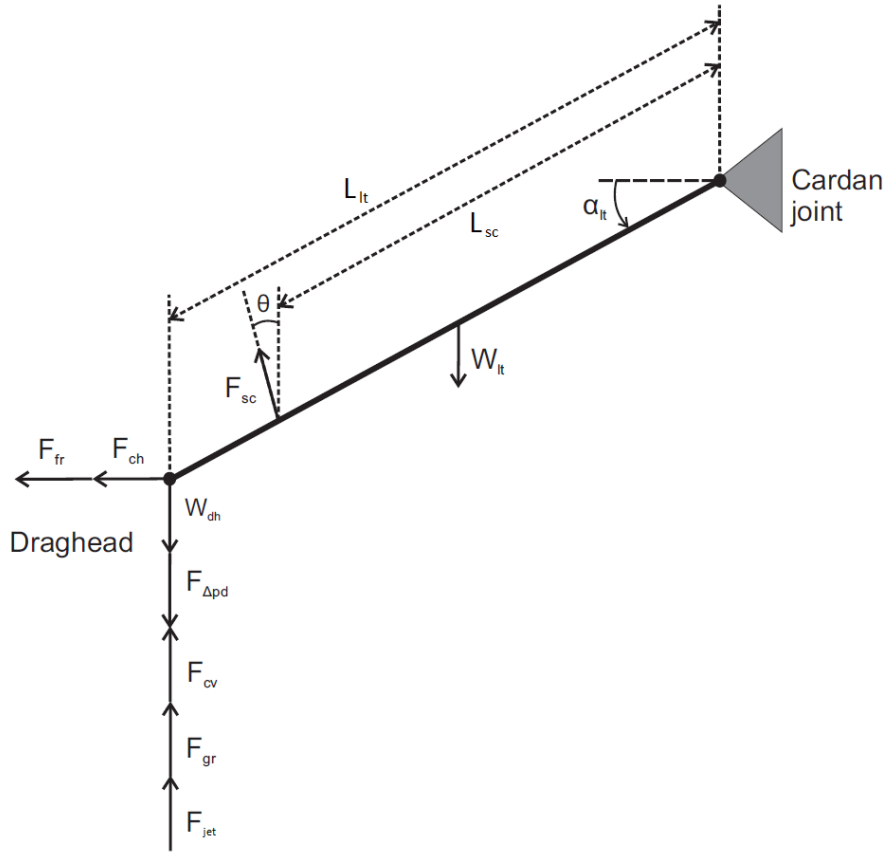


Figure 3.12: Forces acting on the draghead and the lower suction pipe, source: [?]

The weight of the draghead W_{dh} , the lower tube W_{lt} and the sand mixture W_{mix} in the lower tube result in a moment around the cardan joint. Since all components are submerged, the submerged weights need to be used, which are less than the dry weights. The resulting moment is determined as follows:

$$W_{mix} = g(\rho_{mix} - \rho_{water})L_{lt}r_{lt}^2\pi \quad (3.50)$$

$$M_g = \cos(\alpha_{lt})\left(\frac{1}{2}L_{lt}(W_{mix} + W_{lt}) + L_{lt}W_{dh}\right) \quad (3.51)$$

The cable of the swell compensator creates an upwards moment on the lower tube. The oil pressure in the swell compensator is measured and this is used to determine the force. The angle of the cable θ is determined using the position, lengths and angles of the upper and lower tubes.

$$F_{sc} = \frac{1}{2}A_{sc}p_{sc} \quad (3.52)$$

$$M_{sc} = L_{sc} \cos(\theta - \alpha_{lt})F_{sc} \quad (3.53)$$

The pressure difference in the draghead created by the dredgepump results in a vacuum force. This force applies on the opening of the visor, which is w_{dh} wide and has a length of L_{bot} .

$$M_{\Delta p} = L_{lt} \cdot F_{\Delta p} \quad (3.54)$$

$$F_{\Delta p} = \Delta p \cdot w_{dh} \cdot L_{bot} \quad (3.55)$$

The jets in the heel create an impulse force on the tube. The pressure of the jetpump output is measured. With the pressure, the impulse force is determined which pushes the draghead upwards using Bernoulli. The kinetic energy of the water in the pipe is neglected, but some pressure loss is

included because of the friction during transport from the jetpump to the jets.

$$p_{jet} = \frac{1}{2}\rho v^2 \quad (3.56)$$

$$F_{jet} = \rho A v^2 \quad (3.57)$$

$$F_{jet} = 2n \cdot A_{jet}(p_{jetpump} - p_{losses}) \quad (3.58)$$

The moments around the cardanjoint of the lowertube are determined as can be seen in Figure 3.13. The gravity exert the largest moment around the cardan joint and fluctuates slightly due to the varying mixture density in the suction tube. The pressure difference also exerts a large moment and fluctuates even more.

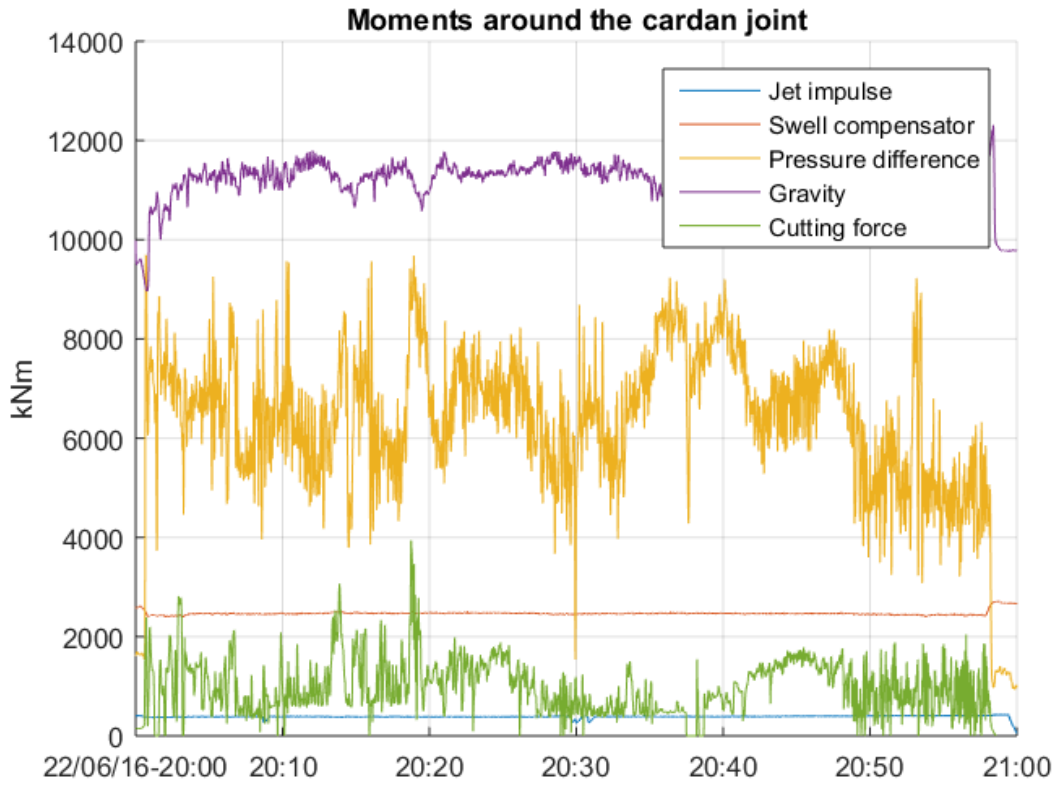


Figure 3.13: Moments around the cardan joint during dredging

Using the assumption of a static equilibrium again, the resulting moment around the cardan joint should be zero. By adding up all moments and using $\sum M = 0$, the remaining moment is assigned to the force on the heel. This assumption is made since we are only interested in the slow dynamics. The angle of the friction force on the heel θ_{heel} must be determined empirically. Based on a steel/sand friction angle of about 30° and additional friction resulting from bulldozing of the heel, an angle of 45° is assumed. This value is uncertain since bulldozing is difficult to model. With the angle, the horizontal component of the heel force is determined.

$$M_{heel} = M_g + M_{sc} + M_{\Delta p} - M_{jet} - M_{cut} \quad (3.59)$$

$$F_{heel} = \frac{M_{heel}}{L_{lt} \cos(\alpha_{lt} - \theta_{heel})} \quad (3.60)$$

$$F_{heel.h} = F_{heel} \sin(\theta_{heel}) \quad (3.61)$$

3.2.3 Validation

After modelling the trail force by adding the horizontal components of the expected forces on the cutting blade and the heel, the accuracy is validated by comparing the modelled trail force with a measurement. The trail force is measured during sea trials using sensors at the suction pipes, see Figure 3.14. The elongation in the strain gauges is used to determine the force in the pipe.



Figure 3.14: Mounted force sensors on the suction tube of the TSHD: 'Chang Jiang Kou', source: IHC

Using Hooke's law and the area of the pipe's cross section A_{pipe} , the force in the pipe is determined:

$$F_{pipe} = A_{pipe} \cdot E_{steel} \cdot \bar{\epsilon} \quad (3.62)$$

Where the average elongation in the pipe $\bar{\epsilon}$ is determined after taking into account the preload of the mounted sensors:

$$\bar{\epsilon} = \frac{(\epsilon_{PS} - \epsilon_{PS0}) + (\epsilon_{SB} - \epsilon_{SB0})}{2} \quad (3.63)$$

Because we are interested in the forces in the horizontal plane, the force in the pipe needs to be correct for the vertical angle of the pipe where the gauges are mounted on.

$$F_{trail} = F_{pipe} \cos(\alpha_{tube.ver}) \quad (3.64)$$

The modelled trail force is compared with the measurement in Figure 3.15.

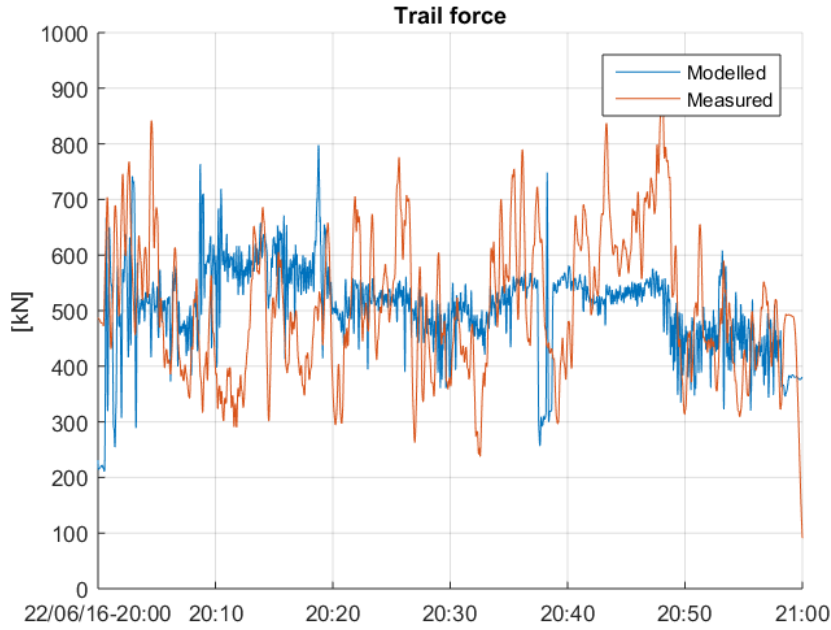


Figure 3.15: Modelled and measured trail force during a seatrial

It shows that the modelled trail force approaches the measurement well and shows similar dynamics. However, the signal shows an offset as well several times. The following reasons are considered to be the main cause of these offsets:

- The visor cylinders are at their lowest position, so their force can not be determined based on the oil pressures. Because relatively loose sand is dredged during the measurements, the visor cylinders reach there lowest position frequently.
- Bulldozing occurs in the heel, which increases the friction of the heel significantly.

To quantify the performance of the modelled trail force, the Variance Accounted For [?] and the Root Mean Square Error are obtained, see Table 3.4.

Table 3.4: Performance of the modelled trail force, calculated for data between 20:00 and 21:00

VAF:	92.5 %
RMSE:	144 kN

The trail force model requires the following signals and parameters to be available:

- 9 measurement signals, as listed in Table 3.3.
- 17 geometrical parameters from drawings
- 12 parameters guessed or approximated

Some parameters can be read directly from technical drawings and we can be sure that these values are correct. Other parameters need to be approximated from technical drawings, created plots or experience. It is expected that these do not differ much from reality, but it still contains uncertainty. The parameters with the highest uncertainty are:

- r_{weight} : the position of the center of mass of the visor
- θ_{heel} : the angle of the friction force between the heel on the bottom
- r_{teeth} : the position of the center of pressure of the cutting force on the teeth

Chapter 4

Estimator design

In the previous chapter, a model of the trail force is explained. It shows that the trail force can be modelled by using the model in combination with position, pressure and density measurements from the draghead and suction pipe. The modelled trail force approaches the measured trail force reasonably well. However, this method is not perfect and it will never be due to inaccurate parameter values, measurement noise and unmodelled dynamics. Therefore, an estimator is built which corrects the modelled trail force and delivers a more accurate estimation of the trail force. The current is also estimated since this disturbance is not measured. The structure of the estimator is shown in Figure 4.1.

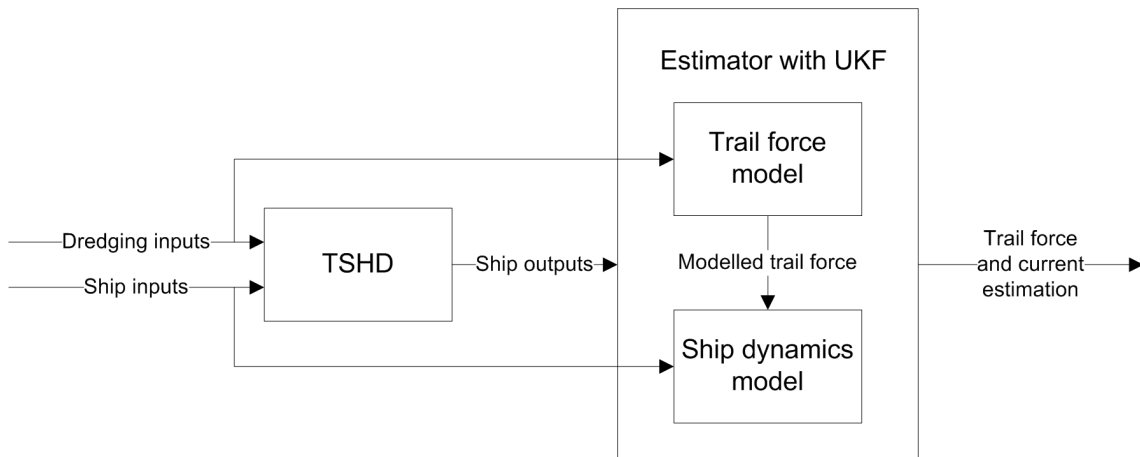


Figure 4.1: Structure of the estimator

The estimations are made using a model of the ship dynamics and the measured outputs. Using the dredging inputs, the modelled of the trail force is obtained. This is then used by the ship dynamics model together with the ship inputs to predict the motion of the ship. With the predicted motion and the ship outputs from the GPS and the compass, the trail force and the current are estimated. By using both models, information about the processes in the draghead is combined with information about the forces and the motion of the ship.

In this chapter it is explained how the current and the trail force are estimated. The unscented Kalman filter is used as an algorithm for the estimator. This choice is justified and the algorithm is explained in Section 4.1. Before describing the complete estimator in Section 4.3, first the working principle of a basic version is explained in Section 4.2.

4.1 The unscented Kalman filter

The Kalman filter is a commonly used algorithm for state estimation. Because the model contains nonlinearities as described in Chapter 3, a linear Kalman filter is not suited. To be able to deal with the nonlinearities, several alternatives are developed as explained by Maskell [?] and Van der Merwe [?]:

- The extended Kalman filter (EKF)
- The unscented Kalman filter (UKF)
- The particle filter (PF)

According to [?], the UKF is more accurately as the EKF for nonlinear systems. The EKF is first order (Taylor series expansion) accurate and the UKF is at least second order accurate. This is even third order for gaussian noise, see [?]. Yet, it is about just as complex as EKF. The UKF does not need to use Jacobians like the EKF does, but uses several datapoints instead. This requires the system functions to be called multiple times each timestep. At the other hand, it is not needed to perform the linearisation with the Jacobians. A visualisation of the covariances approximations by both methods is given in Figure 4.2. It can be seen that the EKF and the UKF estimate the mean and the covariance differently. For this example, the UKF delivers a more accurate estimation of the mean and the covariance than the EKF does.

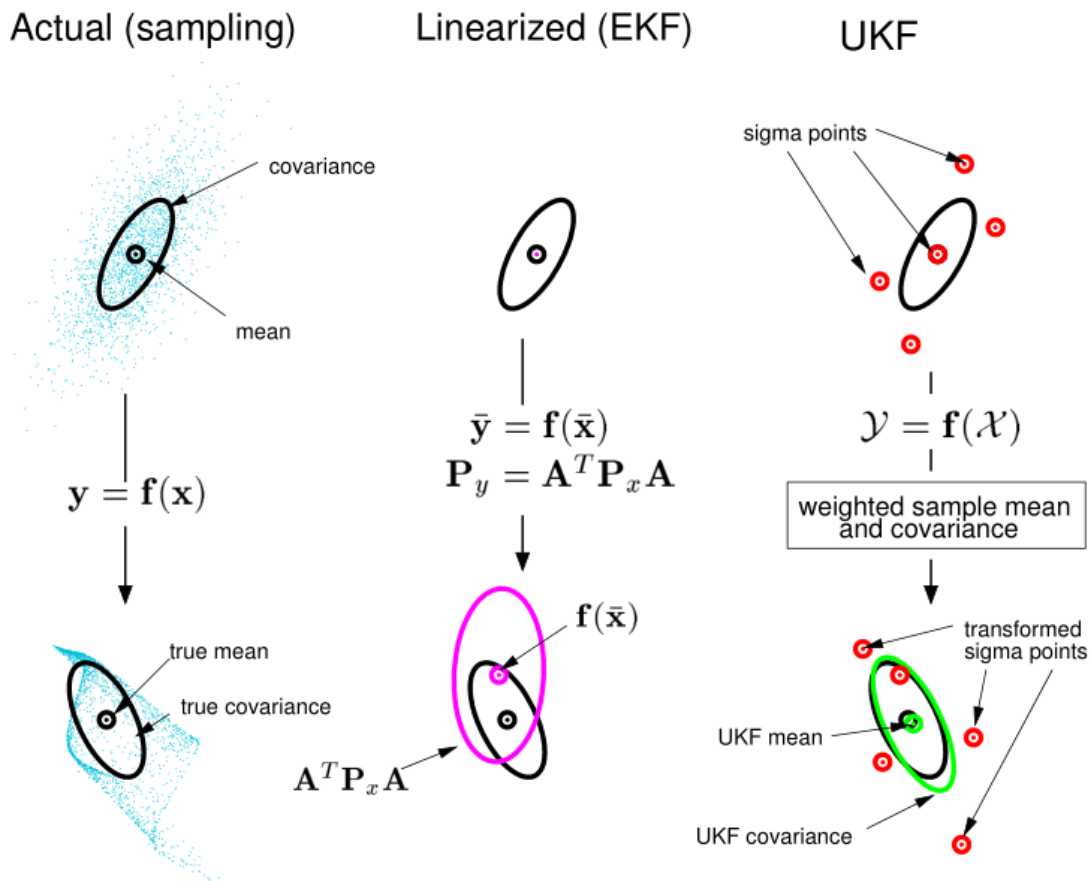


Figure 4.2: Example of actual (a), linearised (b) and UKF (c) covariance propagation, source [?]

The PF uses particles to make a discrete approximation of the probability density functions (pdf) of the state estimations. All particles are propagated through the model functions to track the

course of the states. For high nonlinearities or noise with multimodal pdf's, the PF will give a better estimate than the UKF if enough particles are used. The PF will not be a good filter for models with a high model order, since accurate estimation will then cost a lot of computational power. The estimator model of the TSHD needs 8 states and the noise is not expected to have high nonlinearities or multimodal pdf's. Therefore, it is expected that the advantages of the PF do not outweigh the disadvantages and the UKF is the most promising to use as an estimator for the TSHD. It is able to deal with the nonlinearities and uncertainties in the processes of the TSHD and it is relatively simple to implement.

Working principle

The following nonlinear system, with additive process and measurement noise is taken:

$$x_{k+1} = f(x_k, u_k) + w_k \quad \text{with } w_k \sim (0, Q) \quad (4.1)$$

$$y_k = h(x_k) + v_k \quad \text{with } v_k \sim (0, R) \quad (4.2)$$

With a state estimation \hat{x} and the corresponding covariance matrix P_{xx} available from the previous time step, the UKF derives a new estimation of the state and its covariance using the unscented transform [?]. This method distributes a set of sigma points around the state estimate based on its covariance. After propagating all sigma points through the model, the mean and covariance of the next state is recovered. The following parameters are set during the initialising of the filter to for the distribution of sigma points and the recovering of the mean and covariance, see the pseudo-script below:

Initialising the unscented Kalman filter

Parameters determining the scales of the unscented transform	
$\alpha \in (0, 1]$	determines the spread of the sigma points around the mean
$\kappa \geq 0$	secondary scaling parameter
$\lambda = \alpha^2(n + \kappa) - n$	spread of the sigma points
$\beta = 2$	shape of the expected pdf of x, 2 is optimal for Gaussian distribution
Weights for the means and covariances	
$W_m^{[0]} = \frac{\lambda}{n + \lambda}$	
$W_c^{[0]} = \frac{\lambda}{n + \lambda} + (1 - \alpha^2 + \beta)$	
$W_m^{[i]} = W_c^{[i]} = \frac{1}{2(n + \lambda)}$	for $i = 1, \dots, 2n$

Often, $2n + 1$ sigma points are created, where n is the model order size. All sigma points are propagated through the nonlinear functions, which gives the sigma points of the new state and output. Together with the weights W_m and W_c for the mean and covariance, the predicted new means and covariances are recovered. In [?] it is explained how the weights are determined. The prediction step is shown in the following pseudo-script:

Prediction step of the unscented Kalman filter

Distribute sigma points around the estimated state

$$\begin{aligned}\chi_{k-1}^{[0]} &= \hat{x}_{k-1} \\ \chi_{k-1}^{[i]} &= \hat{x}_{k-1} + \left(\sqrt{(n+\lambda)P_x} \right)_i \quad \text{for } i = 1, \dots, n \\ \chi_{k-1}^{[i]} &= \hat{x}_{k-1} - \left(\sqrt{(n+\lambda)P_x} \right)_{i-n} \quad \text{for } i = n+1, \dots, 2n\end{aligned}$$

Propagate sigma points through system

$$\begin{aligned}\chi_k &= f(\chi_{k-1}, u_{k-1}) \\ \mathcal{Y}_k &= h(\chi_k)\end{aligned}$$

Compute transformed means of states and output as a priori estimates

$$\begin{aligned}\hat{x}_k^- &= \sum_{i=0}^{2n} W_m(i) \chi_k \\ \hat{y}_k^- &= \sum_{i=0}^{2n} W_c(i) \mathcal{Y}_k\end{aligned}$$

Compute covariance matrices

$$\begin{aligned}P_x^- &= \sum_{i=0}^{2n} W_c(i) (\chi_k(i) - \hat{x}_k^-) (\chi_k(i) - \hat{x}_k^-)^T + Q \\ P_y &= \sum_{i=0}^{2n} W_c(i) (\mathcal{Y}_k(i) - \hat{y}_k^-) (\mathcal{Y}_k(i) - \hat{y}_k^-)^T + R \\ P_{xy} &= \sum_{i=0}^{2n} W_c(i) (\chi_k(i) - \hat{x}_k^-) (\mathcal{Y}_k(i) - \hat{y}_k^-)^T\end{aligned}$$

From the resulting means and covariances of the estimated states and outputs, the Kalman gain is derived. The Kalman gain corrects the predicted state with the measurement y_k . This is done to reduce the variance of the state estimate error. The Kalman gain will be high if Q is high and R is low, since it will trust the measurements more than the predicted state. This will result in a fast and aggressive state correction. If Q is low and R is high, the gain will be low. It will trust the state estimate more than the measurements, which results in a slow and smooth response. With the updated state estimate and the Kalman gain, the output estimate and state covariance are updated. The pseudo-script which describes the update step of the UKF algorithm is shown below:

Update step of the unscented Kalman filter

Compute the Kalman gain:

$$K = P_{xy} P_y^{-1}$$

Update the state estimate and output:

$$\begin{aligned}\hat{x}_k &= \hat{x}_k^- + K(y_k - \hat{y}_k^-) \\ \hat{y}_k &= h(\hat{x}_k)\end{aligned}$$

Update the state covariance matrix:

$$P_x = P_x^- - K P_{xy}^T$$

4.2 One dimensional estimator

In this section, the working principle of the estimator is explained. Because of the large number of states and inputs of the estimator, it is difficult to build the complete estimator directly. Therefore, a simplified estimator is built first. The ship dynamics model which is used by the simplified estimator has the following properties:

- The motion and forces of the ship are in surge direction only, so 1D.
- There is no current.
- It has a 100% accurate model of the trail force available.

With these assumptions, the ship motion is modelled.

4.2.1 State equations

The estimator requires the model equations to be in a state space structure:

$$\frac{d}{dt}x = f(x, u) \quad (4.3)$$

$$y = h(x) \quad (4.4)$$

The velocity of the ship and a correction factor for the modelled trail force are used as a state, see Table 4.1. The velocity is an output as well since there is a velocity measurement available from the the simulation model, see Table 4.2.

Table 4.1: States for the estimator model

State	Description
v_{ship}	ship speed
c_F	trail force correction factor

Table 4.2: Output for the estimator model

Output	Description
v_{ship}	ship speed

The velocity is predicted by calculating the forces on the ship and using Newton's second law of motion. With the velocity measurement from the GPS and the predicted velocity, the Kalman filter computes the optimal velocity estimate. By including the correction factor for the trail force as a state, the estimator is able to correct the force when the suggested trail force model does not agree with the measured ship motion.

$$\frac{d}{dt} \begin{bmatrix} v_{ship} \\ c_F \end{bmatrix} = \begin{bmatrix} m^{-1}(F_{trail} + F_{thr} + F_{drag}) \\ 0 \end{bmatrix} \quad (4.5)$$

The forces on the ship can be determined as shown below. The derivations of these forces are treated in Section 3.1.

$$F_{trail} = -c_F \cdot F_{tr.modelled} \quad (4.6)$$

$$F_{drag} = -|v_{ship}| \cdot v_{ship} \cdot (c_{x.min} + \frac{c_{x.max} - c_{x.min}}{m_{sf} - m_{se}}(m - m_{se})) \quad (4.7)$$

$$F_{thrust} = c_1 \cdot |\omega| \cdot |\phi|^{c_2} \cdot (c_3 \cdot \omega \cdot \phi - v_{ship}) \quad (4.8)$$

To be able to calculate the trail force, thrust force and drag force, the signals as shown in Figure 4.3 are required as input for the estimator.

Table 4.3: Input signals for the estimator model

Input	Description
$F_{tr.modelled}$	modelled trail force
m	ship mass
ω	propeller rmp
ϕ	propeller pitch

With these forces, the differential equations (Equation 4.5) are created. The set of equations is then discretised using the Runge-Kutta 4th order method. This is an efficient method which needs to execute the function 4 times every timestep. Since the motion control of the TSHD is executed at 20 Hz, a sample time of $T_s = 0.05$ s is chosen here as well. This is expected to be fast enough to observe the slow dynamics of the ship. The discrete state space function which will be used for the filter has the following structure:

$$x_{k+1} = f(x_k, u_k) + w_k \quad \text{with } w_k \sim (0, Q) \quad (4.9)$$

$$y_k = h(x_k) + v_k \quad \text{with } v_k \sim (0, R) \quad (4.10)$$

The process noise w_k represents the uncertainty of the model, resulting from parameter uncertainty and unmodelled dynamics. In Appendix B, the script is shown where the forces are obtained.

4.2.2 Working principle

The estimator is now implemented into a detailed simulation model of the TSHD (see Appendix A) to test the estimator. Since this estimator assumes the ship motion is limited to 1 direction, the sideways and rotational motions of the simulated ship are blocked. To simulate the GPS, sensor noise is added to this simulated velocity signal. The motion of the ship and the excavation process is first stabilised before estimating, so the estimator is started after 30 seconds. To investigate if the states of the estimator converge to the desired values, the trail force correction factor is given an offset. The following settings are used:

$$R = \mathbb{E}[v_k v_k^T] = 10^{-3} \quad \text{with } y = [v_{ship} \quad \text{[m/s]}] \quad (4.11)$$

$$x_0 = \begin{bmatrix} 1 \\ 1.2 \end{bmatrix} \quad Q = \mathbb{E}[w_k w_k^T] = \text{diag} \begin{bmatrix} 10^{-7} \\ 10^{-6} \end{bmatrix} \quad P_0 = 100 \cdot Q \quad \text{with } x = \begin{bmatrix} v_{ship} & \text{[m/s]} \\ c_F & [-] \end{bmatrix} \quad (4.12)$$

The results are shown in Figure 4.3.

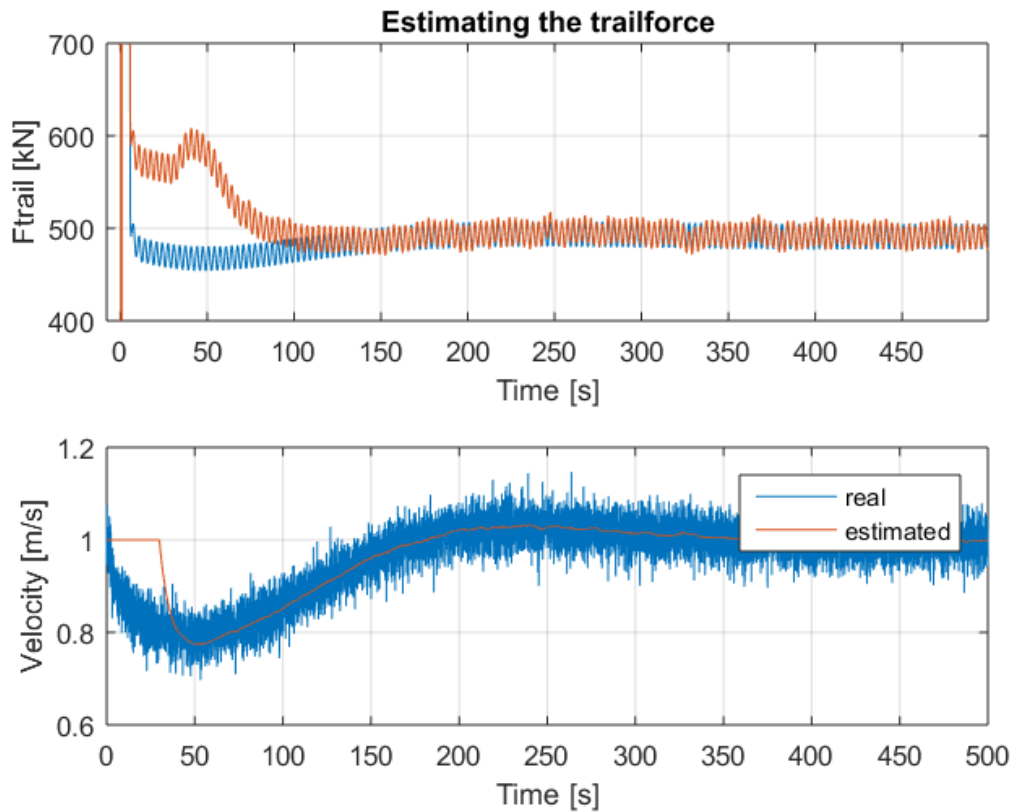


Figure 4.3: Trail force estimation on a simulation of a simplified TSHD

It shows that the estimator is able to work with a noisy velocity signal. The provided modelled trail force in combination of an initial correction factor of $c_F = 1.2$ is higher than the actual trail force, on purpose. When starting the estimator after 30 seconds, this is noticed by the estimator as well. As a result, it slowly decreases this correction gain until the trail force of the ship model in the estimator corresponds with the actual trail force in the simulated ship. Note that since the modelled trail force is here taken equal to the real trail force, the correction gain converges to 1. In reality, the real trail force is not known for the estimator and an imperfect model needs to be used.

4.3 Two dimensional estimator with current

Now, the estimator is extended to 2 dimensions. The model in the estimator has the following properties:

- The motion and forces are in the horizontal plane, so two dimensional and three degrees of freedom
- Two dragheads, trail forces and pipe angles
- There is current
- It has a modelled trail force available for both dragheads.

To model the motion of the ship, the velocities in all three degrees of freedom are required as states. The heading of the ship is needed as well, which leads to 4 states for the motion of the TSHD. To estimate the disturbance, 4 parameters are used as additional states: 2 for the trail force correction gains and 2 to describe the current. This way, the filter is able to correct these values when needed. All 8 states are listed in Table 4.4.

Table 4.4: States for the estimator model

State	Description
v_x	forward ship speed
v_y	sideways ship speed
$\dot{\psi}$	heading rate
ψ	heading
$c_{F.sb}$	trail force correction factor for starboard
$c_{F.ps}$	trail force correction factor for portside
v_{cN}	current speed in North direction
v_{cE}	current speed in East direction

Since not all the states are directly measured, the outputs of the model need to be created so the measurements can be compared with the outputs of the estimator. The signals in Table 4.5 are available from the GPS and the compass of the ship.

Table 4.5: Output signals for the estimator model

output	description
SOG	speed over ground
COG	course over ground
ψ	heading

The velocity of the ship in the local x-y coordinates (which are shown in Figure 4.4 in green) is translated into the measured outputs (which are in red).

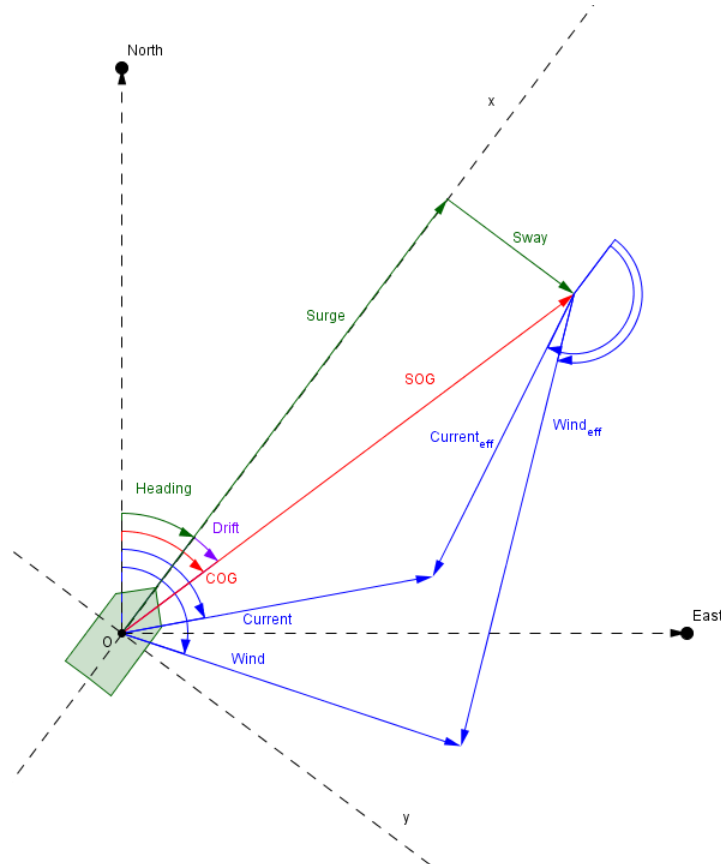


Figure 4.4: Angle and velocity definitions

The velocities are modelled by applying the trail force, thrust forces (main propellers and bow thrusters) and drag force on the mass of the ship. This is done in a similar way as done in Section 4.2.1. The forward (x), sideways (y) and rotational (ψ) components of the forces need to be obtained. With these forces, the differential equations are derived:

$$\frac{d}{dt} \begin{bmatrix} v_x \\ v_y \\ \psi \\ \psi \\ C_{F.sb} \\ C_{F.ps} \\ v_{cN} \\ v_{cE} \end{bmatrix} = \begin{bmatrix} M^{-1} \begin{bmatrix} F_{tr.x} + F_{thr.x} + F_{drag.x} + F_{bow.x} \\ F_{tr.y} + F_{thr.y} + F_{drag.y} + F_{bow.y} \\ M_{tr.\psi} + M_{thr.\psi} + M_{drag.\psi} + M_{bow.\psi} \end{bmatrix} \\ \dot{\psi} \\ 0 \\ 0 \\ 0 \\ 0 \end{bmatrix} \quad (4.13)$$

$$\begin{bmatrix} SOG \\ COG \\ \psi \end{bmatrix} = \begin{bmatrix} \sqrt{v_x^2 + v_y^2} \\ \psi + \arctan(v_y/v_x) \\ \psi \end{bmatrix} \quad (4.14)$$

The differential equation in continuous time is again discretised using the Runge-Kutta 4th order method to obtain the state space model. The derivations of the forces which are used in the estimator model are treated in Section 3.1. An overview of the equations is given below.

$F_{tr.x}$	$= -\cos(\alpha_{tube.sb}) \cdot C_{F.sb} \cdot F_{tr.sb} - \cos(\alpha_{tube.ps}) \cdot C_{F.ps} \cdot F_{tr.ps}$
$F_{tr.y}$	$= \sin(\alpha_{tube.sb}) \cdot C_{F.sb} \cdot F_{tr.sb} - \sin(\alpha_{tube.ps}) \cdot C_{F.ps} \cdot F_{tr.ps}$
$M_{tr.\psi}$	$= y_{inlet} \cdot (\cos(\alpha_{tube.sb}) \cdot C_{F.sb} \cdot F_{tr.sb} - \cos(\alpha_{tube.ps}) \cdot C_{F.ps} \cdot F_{tr.ps}) + x_{inlet} \cdot F_{tr.y}$
$F_{thr.x}$	$= F_{prop.sb} + F_{prop.ps} - 1.6 \cdot \frac{1}{2} \rho_w \cdot C_T \cdot (F_{prop.sb} \cdot \sin(\alpha_{rud.sb})^2 + F_{prop.ps} \cdot \sin(\alpha_{rud.ps})^2)$
$F_{thr.y}$	$= 1.5 \cdot \frac{1}{2} \rho_w \cdot C_T \cdot (F_{prop.sb} \cdot \sin(2 \cdot \alpha_{rud.sb}) + F_{prop.ps} \cdot \sin(2 \cdot \alpha_{rud.ps}))$
$M_{thr.\psi}$	$= y_{rud}(F_{thrust.x.PS} - F_{thrust.x.SB}) - x_{rud}(F_{thrust.y.PS} + F_{thrust.y.SB})$
$F_{drag.x}$	$= -v_r v_r \cdot (c_{x.min} + \frac{c_{x.max} - c_{x.min}}{m_{sf} - m_{se}} (m - m_{se}))$
$F_{drag.y}$	$= -v_r v_r \cdot (c_{y.min} + \frac{c_{y.max} - c_{y.min}}{m_{sf} - m_{se}} (m - m_{se}))$
$M_{drag.\psi}$	$= -\dot{\psi} \dot{\psi} \cdot (c_{y.min} + \frac{c_{y.max} - c_{y.min}}{m_{sf} - m_{se}} (m - m_{se})) \cdot L_{sh}^3 / 32$
$F_{bow.x}$	$= 0$
$F_{bow.y}$	$= F_{max} \cdot (\frac{\omega}{\omega_{max}})^2 \cdot \max(0, (1 - \frac{ v }{5}))^{1.4}$
$M_{bow.\psi}$	$= x_{bow} \cdot F_{bow.y}$

To obtain these forces, the input signals as listed in Table 4.6 are required. Furthermore, all parameters have to be filled in.

Table 4.6: Input signals for the estimator model. Most signals arise from both sides of the TSHD and are therefore double.

input	description
$F_{tr.mod}$	modelled trail force (2x)
α_{tube}	horizontal tube angle (2x)
ϕ	propeller pitch (2x)
α_{rud}	rudder angle (2x)
ω_{prop}	propeller speed (2x)
ω_{bow}	bow thrusters speed
m	ship mass

4.4 Summary

In this chapter, it is explained how the current and trail force estimator is designed. The estimator requires a modelled trail force, a model of the ship dynamics and a filter technique. Because the model of the ship dynamics contains nonlinearities, the commonly used linear Kalman filter is not suited as an algorithm for the estimator. The unscented Kalman filter is used as an alternative.

The estimator makes a real time estimation of the states using a state space system. This is a discretised version of the differential equations as described in Equations 4.13 - 4.14, using the Runge-Kutta 4 method. The following signals are required to be available:

Table 4.7: Signals required for the estimator

category	signal	description
Dredging inputs	α_{lt}	vertical angle of the lower tube
	α_{ut}	vertical angle of the upper tube
	ρ_{mix}	density of the sand/water mixture in the pipe
	p_{jet}	output pressure of the last jetpump
	p_{sc}	pressure in the swell compensator
	$p_{vc.rod}$	pressure in the rod side of the visor cylinders
	$p_{vc.bot}$	pressure in the bottom side of the visor cylinders
	Δp	pressure difference in the draghead
Ship inputs	x_{vc}	position of the visor cylinders
	α_{rud}	rudder angle (2x)
	α_{tube}	horizontal tube angle (2x)
	ϕ	propeller pitch (2x)
	ω_{prop}	propeller rmp (2x)
	ω_{bow}	bow thrusters rmp
Ship outputs	m	ship mass
	SOG	speed over ground
	COG	course over ground
	ψ	heading

The dredging inputs are required for the trail force model. The ship dynamics model uses the ship inputs together with the modelled trail force to calculate all forces on the ship. With these forces, the motion of the ship is predicted. The estimator then compares the measured ship outputs with the predicted motion and corrects the trail force and the current when necessary.

Chapter 5

Estimation results

In this chapter, the performance of the estimator as explained in Chapter 4 is evaluated by using:

- Simulation data
- Measurement data

The simulation model of the TSHD is validated with measurements of the real TSHD as shown in Chapter 3. The performance of the estimator applied on simulation data will therefore be comparable with the performance on a real TSHD. By setting all inputs and settings, a realistic scenario is created for the simulation model. Simulations are useful since several circumstances can be created to examine the working principles and the performance of the estimator. Measurement data is used to show how it performs on an actual ship. However, we are limited to the recorded data from a seatrial. Figure 5.1 shows the test structure and the signals of the estimator.

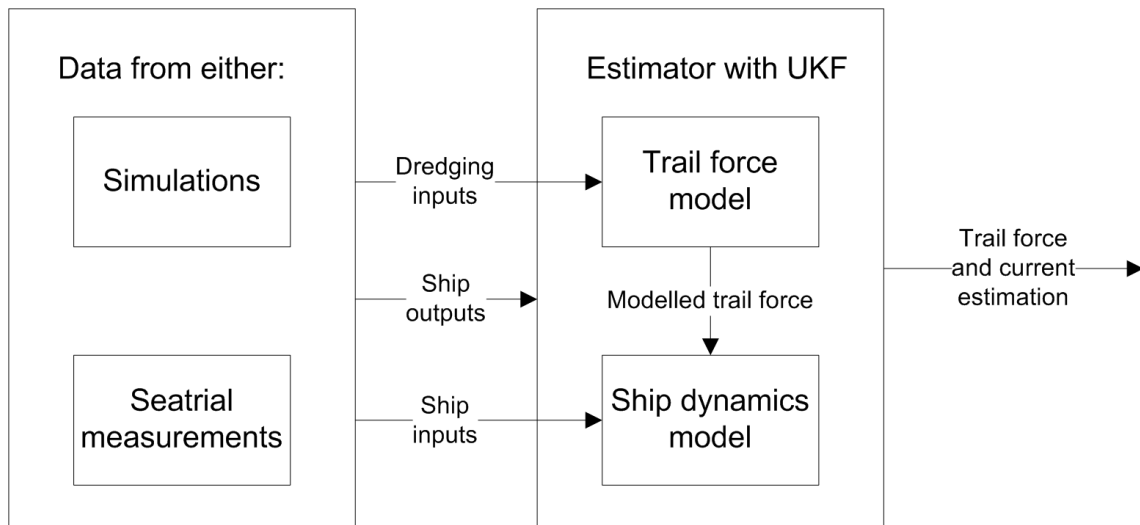


Figure 5.1: Test structure of the estimator

The estimator as explained in Chapter 4 contains the modelled ship dynamics (Section 3.1), the modelled trail force (Section 3.2) and the UKF algorithm (Section 4.1). The signals as listed in Table 4.7 are created using the simulation model of the TSHD with the scenario as explained in Section 5.1. The resulting trail force and current estimates are shown and reviewed here as well. The results of the estimator applied on measurement data are treated in Section 5.2.

5.1 Estimating using simulation data

It is desired to have the simulations as realistic as possible, so the performance of the estimator will be representable for the real TSHD. Measurement data from the seatrial is observed to create realistic input signals for the TSHD. With this scenario, the TSHD is simulated together with the estimator. The resulting trail force and current estimations are compared with the real trail force and current.

5.1.1 Scenario

The trail force is difficult to model since it is related to several processes, like the jetting, the cutting and the erosion in the draghead. Furthermore, sand properties are unknown and the circumstances change constantly. The varying circumstances are reproduced in the simulation by creating a realistic scenario. The actuators of the ship need to ensure the ship motion is realistic so these need to be set as well. In this part, the following signals are set to achieve this:

- dredging depth and sand properties
- visor position
- ship propellers and rudders

Furthermore, other settings as jet pumps, dredge pumps and diesel engines are set to the nominal speed. A small fluctuation is added to the dredge pump speed to represent a varying resistance of the mixture in the tube and the draghead.

Dredging depth and sand properties

In the simulation model, Miedema's cutting theory [?] is used to calculate the cutting force on the blades. Cavitation cutting is assumed since this is often the case during dredging with the usual dredging depth, ship velocity, layer height and sand properties.

$$F_{c.hor} = d \cdot N_t \cdot w_t \cdot \rho_w \cdot g \cdot h_c \cdot (h_z + 10) \quad (5.1)$$

Where d is the cutting force coefficient, N_t the number of teeth, w_t the width of a teeth, ρ_w the water density, g the gravitational constant, h_c is the cutting depth and h_z the dredging depth. The parameters N_t , w_t , ρ_w and g are fixed. A realistic varying trail force is created by varying the following parameters:

- h_z : dredging depth
- k_{si} : permeability of sand
- d : cutting force constant

The permeability of the sand influences the excavation depth by erosion and jetting, this is shown in Figure 2.8. Therefore, the thickness of the layer which is excavated by cutting h_c is influenced by the permeability of the sand k_{si} .

The dredging depth from measurement data is around 25m, so this value is adopted for the simulation as well. To create a realistic varying signal, a sinus signal and low pass filtered zero mean white noise with unit variance is added as shown in Figure 5.2 and the following equation:

$$h_z(t) = 25 + 0.1 \cdot \sin(2\pi t/20) + \left(\frac{1}{30s + 1}\right)^2 \cdot e(t) \quad \text{with } e(t) \sim (0, 1) \quad (5.2)$$

The sinus has a period time of 20s, which corresponds to under water sand dunes of about 20m since the TSHD dredges with about 1m/s.

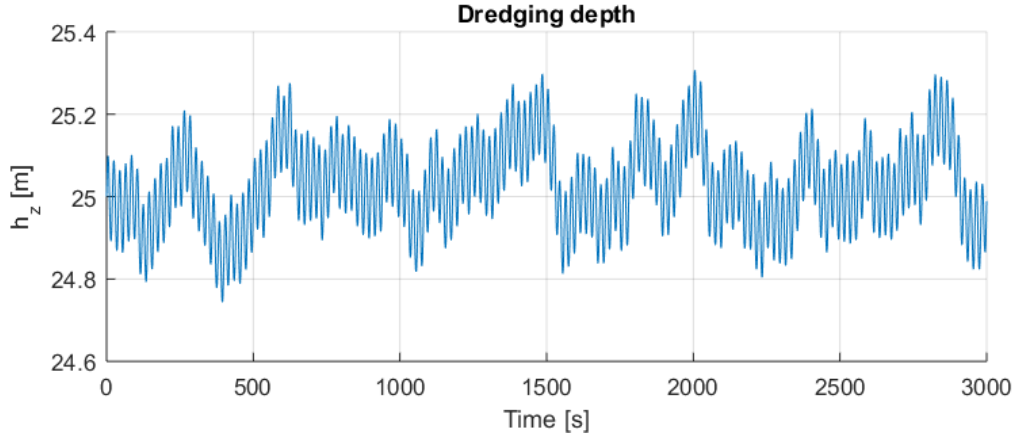


Figure 5.2: The dredging depth during the simulation

The permeability of the sand and the cutting force coefficient depend on type of sand, which changes over time. The cutting force coefficient d from Equation 5.1 depends on 4 parameters according to Miedema:

$$d = f(\alpha_t, h_b/h_i, \phi, \delta) \quad (5.3)$$

The blade angle α_t , blade height cutting height ratio h_b/h_i , the internal sand friction angle ϕ and the sand/steel friction angle δ . A reasonable assumption for sand is that $\delta = 2/3 \cdot \phi$. Furthermore the height ratio is high for high blade angles and low for low blade angles. Now the cutting force coefficient is read from Miedema's tables and only depends on 2 parameters as shown in Table 5.1.

Table 5.1: Cutting force coefficient d with varying blade angles and friction angles

	$h_b/h_i = 1$	$h_b/h_i = 2$	$h_b/h_i = 3$
	$\alpha = 30^\circ$	$\alpha = 45^\circ$	$\alpha = 60^\circ$
$\phi = 32^\circ$	1.5780	2.3852	3.4266
$\phi = 37^\circ$	2.0425	3.1829	4.8142
$\phi = 42^\circ$	2.6437	4.2474	6.7637
$\phi = 47^\circ$	3.4219	5.6678	9.5026
$\phi = 52^\circ$	4.4291	7.5632	13.3507

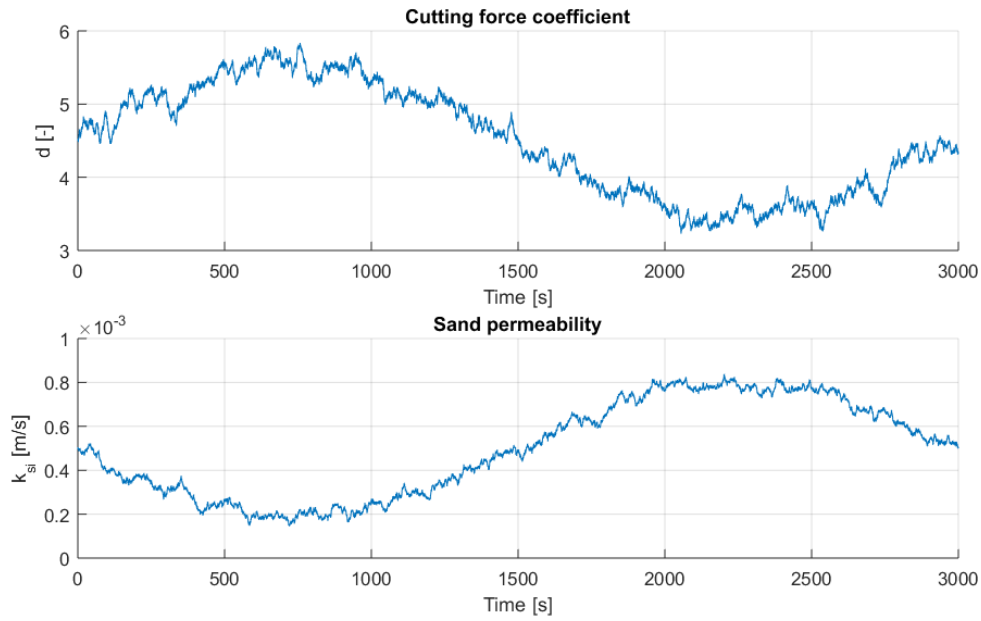
It is expected that a varying value between 3 and 6 is realistic. The type of sand is varied slowly over time, so the following formula is used:

$$d(t) = 4.5 + \sin(2\pi t/3000) + \frac{1}{30s+1} \cdot e(t) \quad \text{with } e(t) \sim (0, 1) \quad (5.4)$$

This represents sand properties that change over time with a period time of 3000 seconds, which is about 3 km when dredging with 1 m/s. The dredged sand from the measurement data is expected to be medium sand, which has a typical grain size of about 300 μm . The permeability of the sand varies between 0.1 and 1 mm/s. Since the cutting coefficient is reversed related to the permeability, a sinus signal with the same frequency as in the cutting force coefficient is used, but this time it is subtracted.

$$k_{si}(t) = 5 \cdot 10^{-4} - 3 \cdot 10^{-4} \cdot \sin(2\pi t/3000) + \frac{0.0002}{30s+1} \cdot e(t) \quad \text{with } e(t) \sim (0, 1) \quad (5.5)$$

Figure 5.3 shows the values of the cutting force coefficient and the permeability over time:

Figure 5.3: The sand parameters d and k_{si} during simulation

Visor control

The position of the visor is either controlled automatically or manually. To achieve a range in dynamics in the draghead, the simulated visor is controlled manually. Every minute, a new random value of the visors position is set. A rate limiter is added to the random step signal to limit the speed of the visor cylinder to 3%/sec. The signal is shown in Figure 5.4. It turns out that the visor cylinder should be between 5 and 25 % upwards to achieve a balance between jetting and cutting. This is explained by Van den Bergh [?] and denoted by (b) in Figure 5.5. A higher visor would result in a gap under the teeth and a bulldozing heel (see a), which are both undesirable for the dredging efficiency. A lower visor will result in a gap under the heel, and therefore reduced jet production and high cutting forces (see c). Since this is undesired as well, the dredging operator or controller will try to stay in the balanced situation. This aspect is included in the simulation as well.

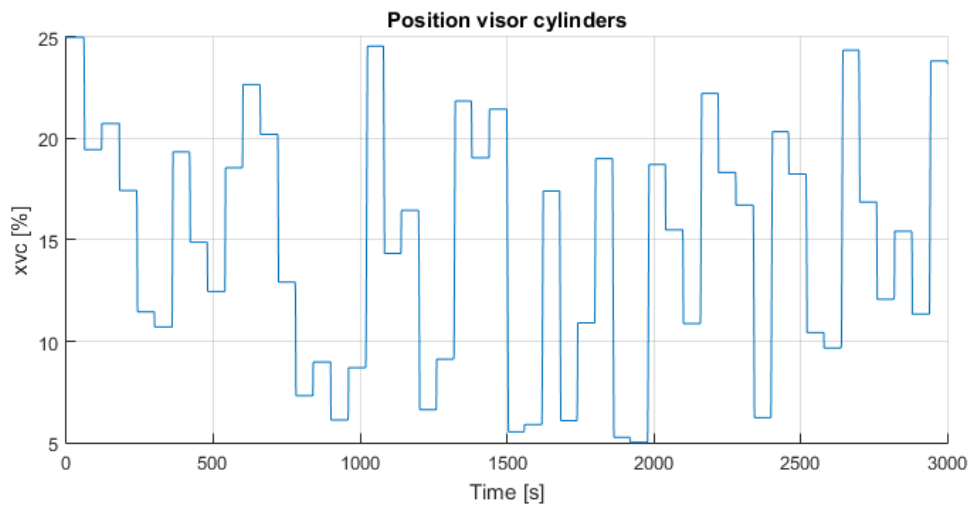
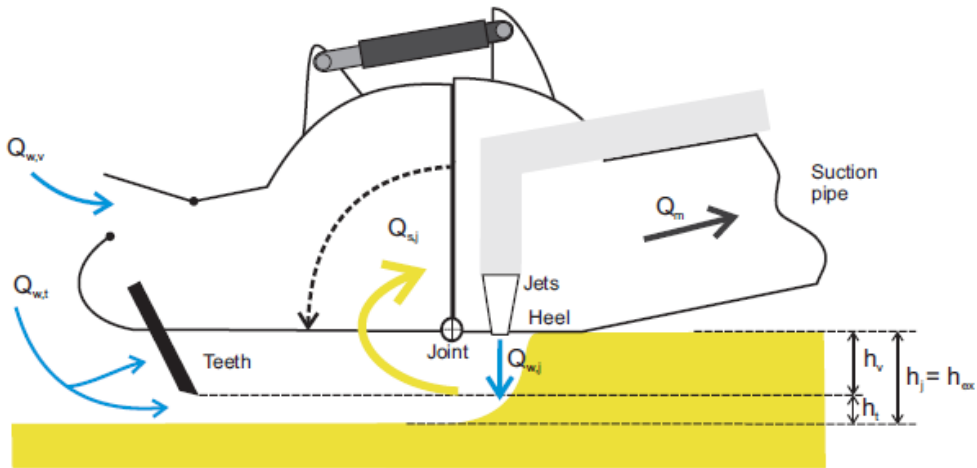
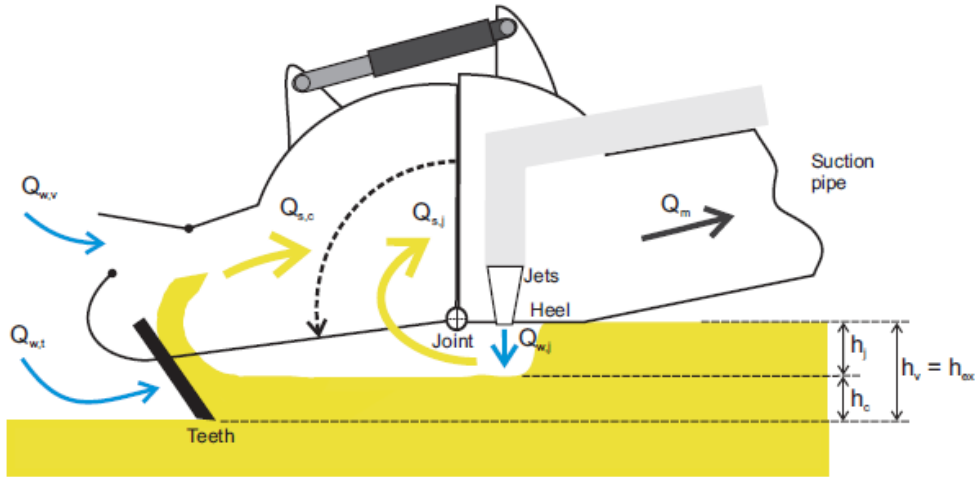


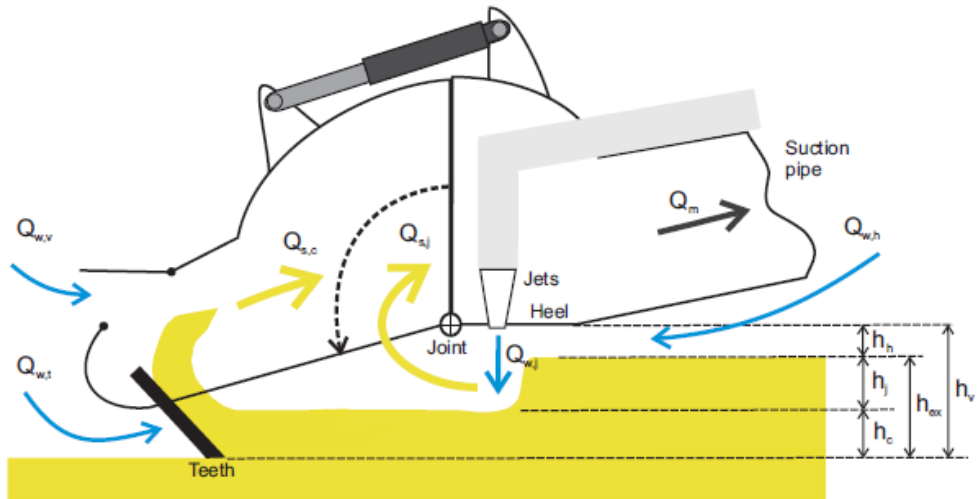
Figure 5.4: Position of the visor cylinders, where the visor is almost down at 5 %.



(a) Excavation regime 1, toe gap: $h_{ex} > h_v$



(b) Excavation regime 2: $h_{ex} \approx h_v$



(c) Excavation regime 3, heel gap: $h_{ex} < h_v$

Figure 5.5: Three excavation regimes, source: [?]

Ship propellers and rudders

The ship motion is controlled in surge and heading direction using:

- propeller pitches
- rudder angles
- bow thrusters speed

The velocity of the ship is required to be maintained around 1 m/s. Because of the fluctuating trail force, it is difficult to achieve a shipspeed around 1 m/s by setting the pitch of the propellers manually. Therefore, a PI controller is used. Both propellers use the pitch signal as shown in Figure 5.6 so they will perform equal thrust forces.

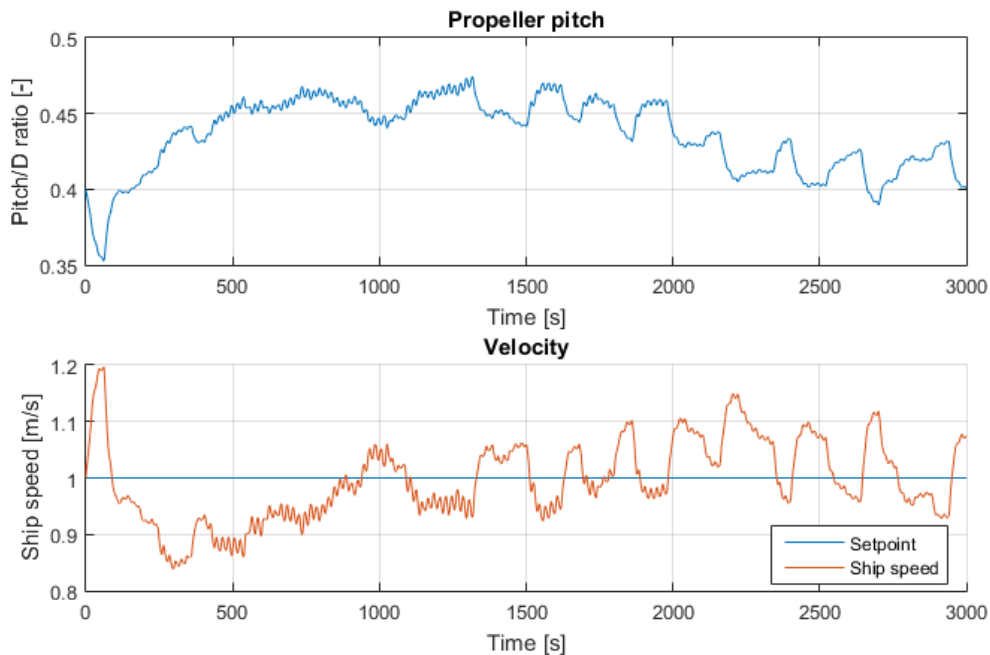


Figure 5.6: Resulting signals as applied on the propulsion actuators of the TSHD

The heading needs to be stabilised with a PI controller as well. The suction pipe inlets are positioned in front of the center of mass of the ship, which would result in an unstable heading of the ship. Furthermore, a sideways current or a difference between the trail forces at the dragheads will turn the ship as well. The controller uses the rudders and bow thrusters to stabilise the heading. An anti windup is used in the controller to improve the performance with a changing setpoint or with saturated actuators. The bow thruster propeller speed and the rudder angles are all controlled with the same steering signal as shown in Figure 5.7. It can vary from a maximal clockwise turn (positive) to a maximal counter-clockwise turn (negative). At 100 %, the bow thrusters are at full speed and the rudders are at 45° . A slow turn is performed by the ship to see what happens to the estimator. This is done while dredging with both dragheads. With the ship moving in rotational direction as well, all parts of the model are affected so several dynamics are observed.

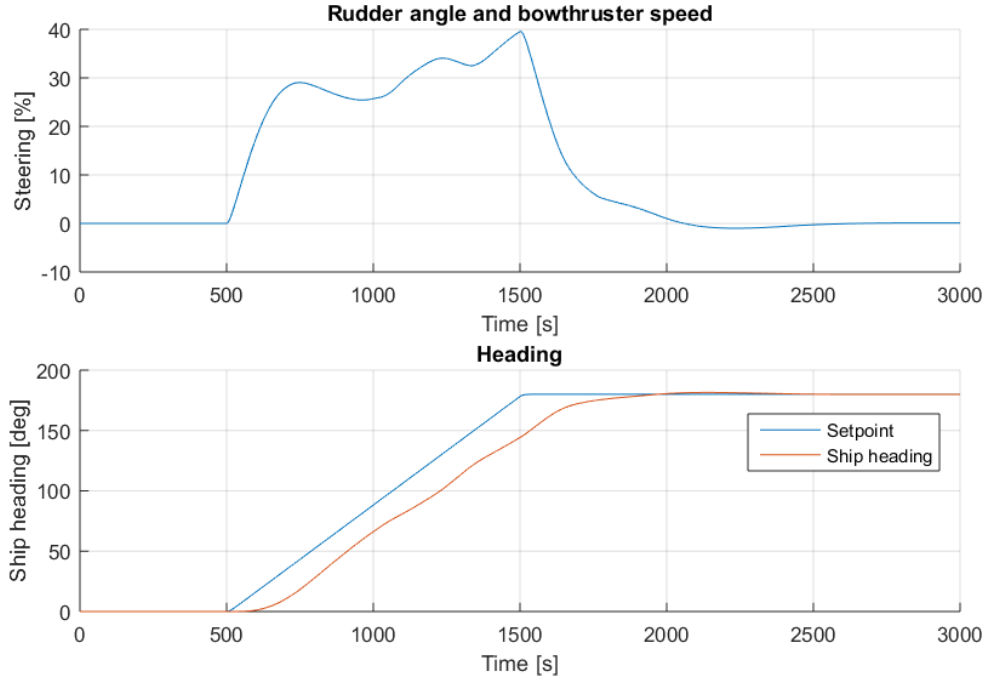


Figure 5.7: Signals applied on the steering actuators of the TSHD

5.1.2 Estimation results on simulations

The scenario as described in the previous section is used to simulate the TSHD with the estimator to observe the performance of the estimator. Noise v with a covariance R is added to the simulated signals y to make them realistic. See Table 4.5 for the definition of the output signals. From measurement data it is observed that the signals contain noise with the variances as shown below. The noise is therefore added to the simulated signals as well.

$$R = \mathbb{E}[vv^T] = \text{diag} \begin{bmatrix} 10^{-3} \\ 10^{-3} \\ 10^{-6} \end{bmatrix} \quad \text{with} \quad y = \begin{bmatrix} SOG & [\text{m/s}] \\ COG & [\text{rad}] \\ \psi & [\text{rad}] \end{bmatrix} \quad (5.6)$$

The variance Q of the process noise w has to be set as well. This noise corresponds to the state equations to represent parameter uncertainty or unmodelled dynamics. By defining the uncertainty of every state equation on the diagonals of the Q matrix, the behaviour of the states in the estimator is tuned. See Table 4.4 for the definition of the states. The initial states of the estimator are chosen about equal to the actual states. The trail force correction gains and current estimates get a small offset to observe the convergence of the estimator. It turns out that using the following initial state x_0 and covariance matrix Q lead to realistic results:

$$x_0 = \begin{bmatrix} 1 \\ 0 \\ 0 \\ 0 \\ 1.2 \\ 1.2 \\ 0 \\ 0 \end{bmatrix} \quad Q = \mathbb{E}[ww^T] = \text{diag} \begin{bmatrix} 10^{-7} \\ 10^{-8} \\ 10^{-9} \\ 10^{-12} \\ 10^{-7} \\ 10^{-7} \\ 10^{-8} \\ 10^{-8} \end{bmatrix} \quad P_0 = 1000 \cdot Q \quad \text{with} \quad x = \begin{bmatrix} v_x & [\text{m/s}] \\ v_y & [\text{m/s}] \\ \psi & [\text{rad/s}] \\ \psi & [\text{rad}] \\ c_{F.sb} & [-] \\ c_{F.ps} & [-] \\ v_{cN} & [\text{m/s}] \\ v_{cE} & [\text{m/s}] \end{bmatrix} \quad (5.7)$$

The TSHD is simulated together with the estimator using the earlier described input signals. The estimator is started after 30 seconds to have the motion of the ship and the excavation process stabilised.

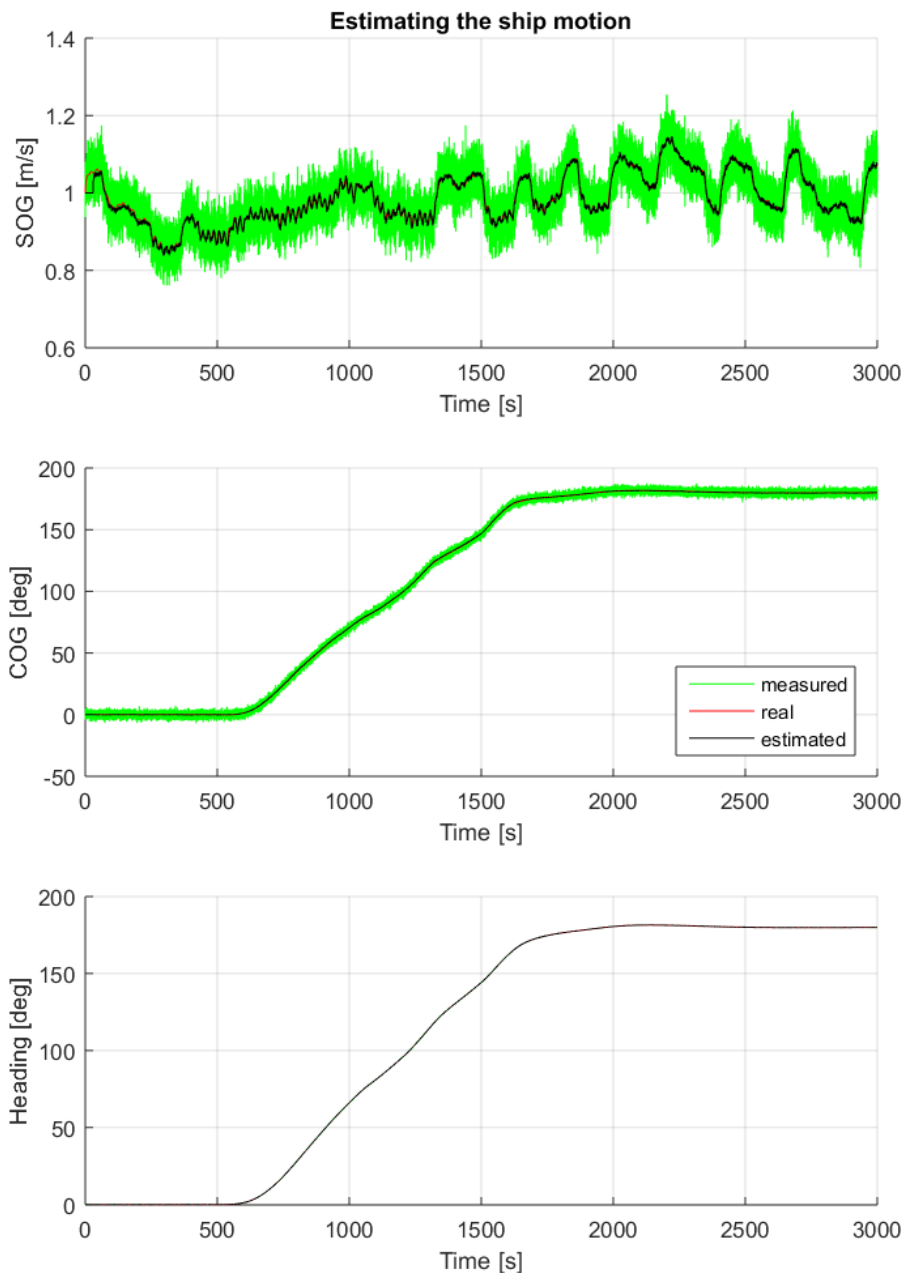


Figure 5.8: Ship motion estimations. Note that the estimations often cover the real signals. Because of the low noise on the heading measurement, this line is covered by the estimation as well.

Figure 5.8 shows that the dynamics in the motion are estimated with a high accuracy for all three outputs, especially the heading since this measurement contains almost no noise. It takes about 30 seconds to eliminate the small offset in the initial speed of the ship, but furthermore there are no significant offsets. This makes sense because these signals are all directly measured. Furthermore, the figure shows that the speed over ground is disturbed by the varying trail force. The need to include a trail force estimation into the ship speed controller is hereby demonstrated as well.

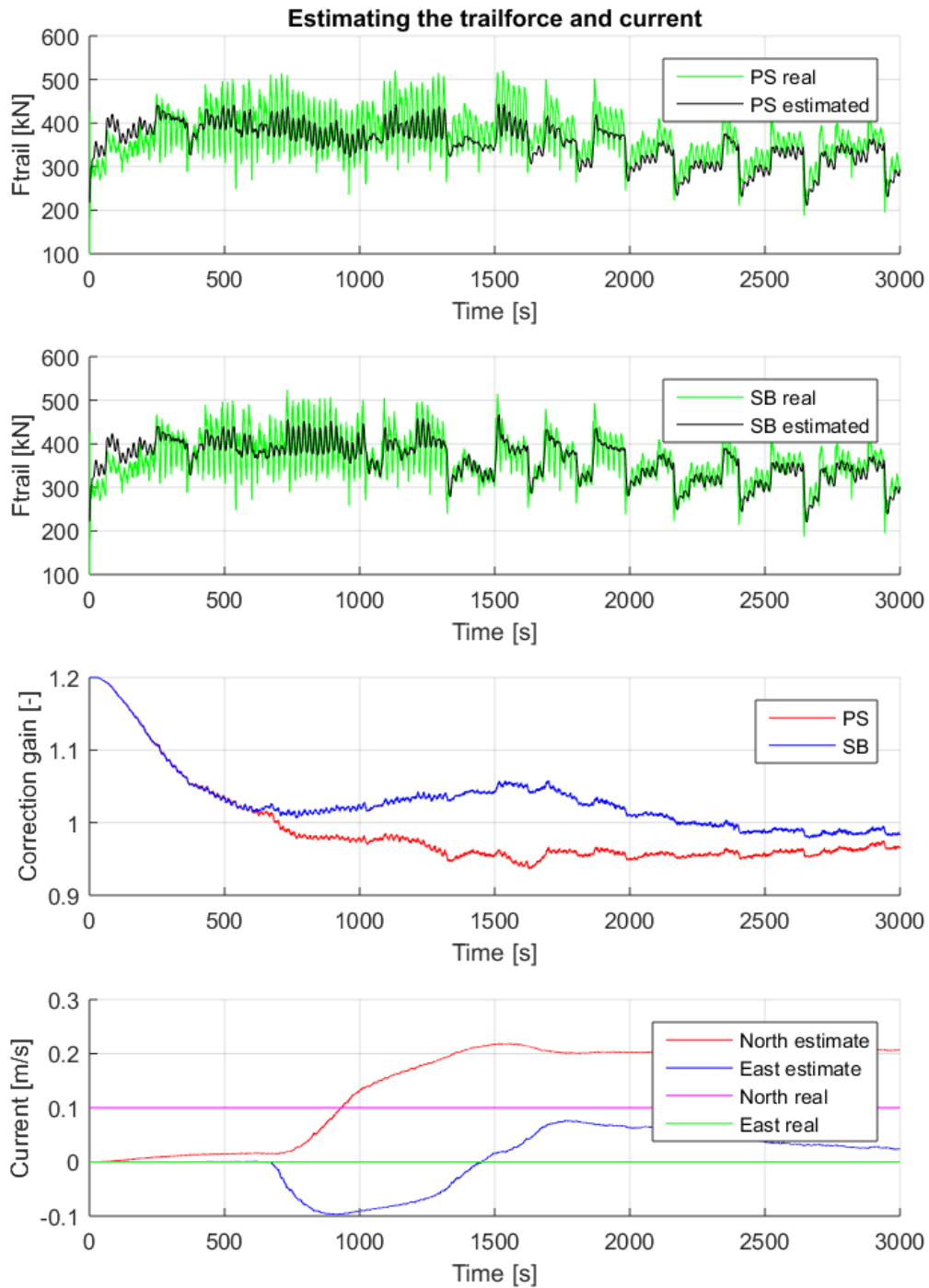


Figure 5.9: Resulting trail force and current estimations

Figure 5.9 shows that the correction gains converge to 1 in about 500 seconds and the low frequency dynamics of the trail force are modelled accurately. The higher frequency dynamics are slightly damped. The first reason is that the estimator uses the pressure measurements of the visor cylin-

ders to determine the cutting force, but the hydraulic system damps these pressures. Secondly, the density of the mixture is measured inside the ship. Therefore, the estimator calculates the weight with a delay of about 8 seconds. Since only the low frequency dynamics are important for the control of the TSHD's velocity, this is not a problem. However, it can be seen that the estimated trail forces have a mismatch of about 5% when the ship makes the U-turn. This is probably because there is some model inaccuracy in the ship moment equilibrium of the estimator. The DP-system of IHC freezes the estimation of the correction gains and the current when the ship makes a turn to prevent this.

Furthermore, the estimator has some difficulties with distributing the correct part of the total disturbance forces to the the trail force and the other part to the current. Because of the small phase delay of the modelled trail force, the estimator fits this with a slightly reduced correction gain and an extra current coming from the front of the ship. Because the inaccuracy of the modelled trail force is limited, this effect causes a mismatch of only a 2 percent on the correction gains and 0.1 m/s on the current estimates. The DP-system of IHC reduces this effect by having the current estimation converge before the dredging is started. When the dredging is started, the current estimation is slowed down so the estimator will focus on estimating the trail force. This works well since the current varies only slightly over time. To quantify the performance of the estimations, the Variance Accounted For [?] and the Root Mean Square Error are obtained, see Table 5.2. Note that these values depend on the chosen scenario and the initial state of the estimator.

Table 5.2: Performance of the estimator when using the trail force model

Performance	VAF	RMSE
Trail force port side	98.8%	41.1 kN
Trail force starboard side	99.0%	37.0 kN
Current estimation	-	0.107 m/s

5.1.3 Comparing the results with the benchmark

To be able to value the performance of the estimator, the currently used method by the DP-system of IHC is simulated as a benchmark. This method uses the pressure difference in the draghead to model the trail force. The TSHD is simulated with the same scenario and the settings of the estimator are set equal as well. The results of the benchmark estimator are shown together with the previously obtained results in Figure 5.10. Only the estimations of the trail force and current are shown, since the estimated motion of the ship does not show anything new. These are directly measured and therefore estimated accurately, just as in Figure 5.8.

The estimation results show that the pressure difference is not able to capture all dynamics in the trail force. Especially between 700 - 1000s, when the pressure in the draghead drops because of a small gap under the heel. Therefore, the estimation does not approach the real trail force as accurately as the new method does. Because the states are estimated with a higher uncertainty, the values in the state estimation covariance matrix (' P_{xx} ') are higher. This makes the state estimations relying more on the measurements, which results in a more fluctuating estimation. To quantify the difference of the performances between both methods, the Variance Accounted For [?] and the Root Mean Square Error are obtained as well for this method, see Table 5.3. The current estimation is not significantly better, but the table confirms that the estimator which uses the trail force model is able to estimate the trail force more accurately than the benchmark.

Table 5.3: Performance of the estimator when using the Δp signal

Performance	VAF	RMSE
Trail force port side	94.3%	88.8 kN
Trail force starboard side	95.3%	80.0 kN
Current estimation	-	0.118 m/s

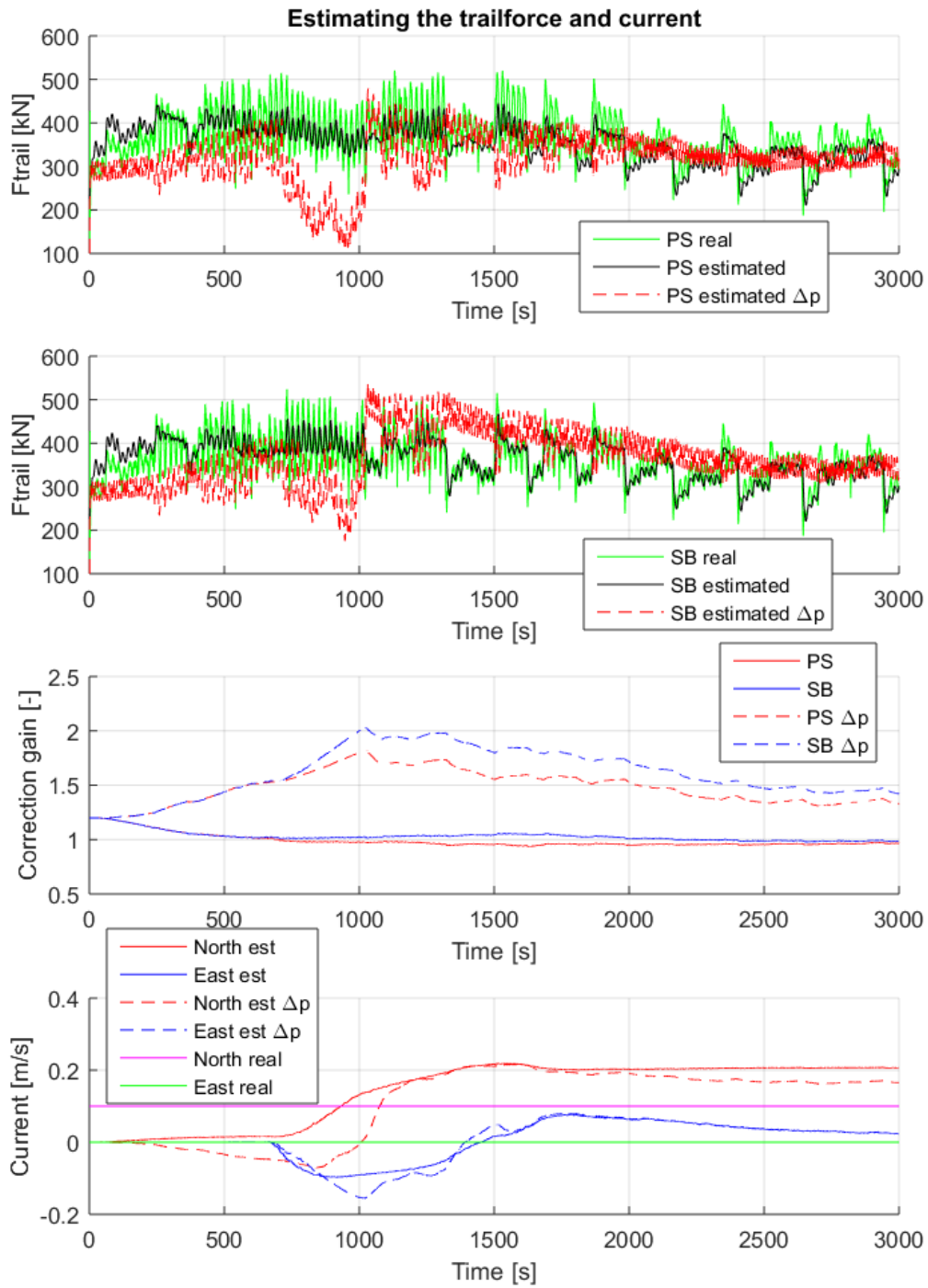


Figure 5.10: Resulting trail force and current estimations in combination with the benchmark (' Δp ') results shown with dashed lines

5.2 Estimating using measurement data from seatrial

In this section, the estimator is applied on measurement data available from a seatrial of the TSHD 'Jun Yang 1'. During several dredging cycles, input and output signals from the TSHD are recorded. These are used for the estimator to test its performance. The force in the suction pipes is measured from which the trail force can be derived, and this is compared with the estimation.

5.2.1 Scenario

Out of several available dredging cycles from 21 to 24 June 2016, the most suitable dredging part is chosen. This data is recorded on 24 June from 16:00 to 16:50. Most recorded signals have a good quality during this period, this is not the case for all periods. Furthermore, the modelled trail force is not always valid.

The motion of the ship is controlled with the propellers, rudders and bow thrusters. The signals are shown in Figure 5.11. The pitch of the propellers do not vary a lot during dredging. Furthermore, mainly the rudders are used to slightly steer the ship.

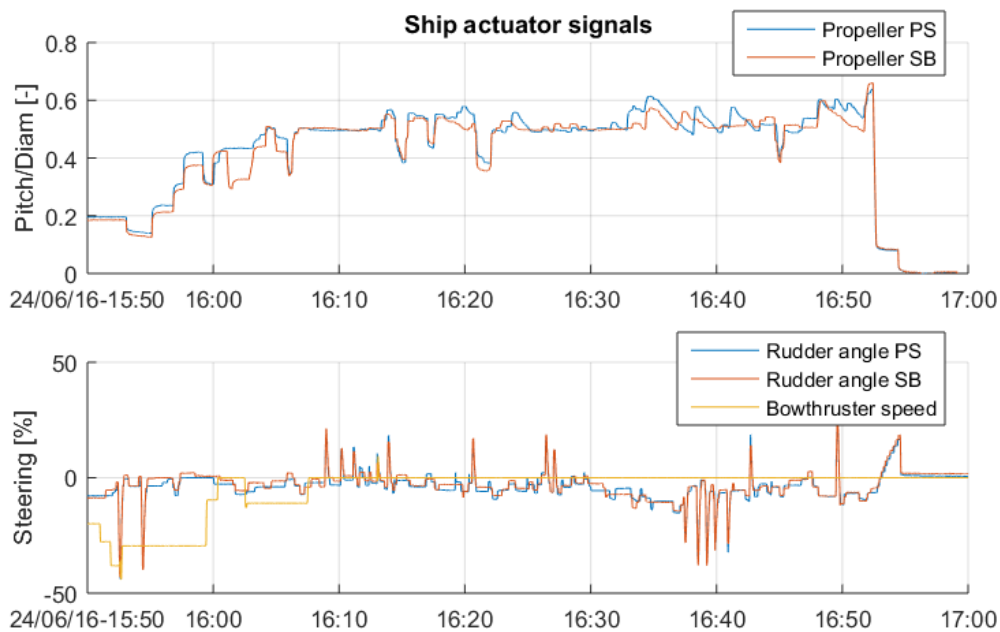


Figure 5.11: Propulsion and steering signals during dredging.

The position of the visor cylinders is shown in Figure 5.12. It shows that the positions are often at their lowest position (0%). This is because the dredged sand is relatively coarse and therefore easy to excavate. Furthermore, the pressures in both sides of the starboard side cylinders are often equal, which means the visor is in 'loose mode'. The visor is set to 'controlled mode' for a short moment a few times as well. The pressures in the port side cylinders are not measured.

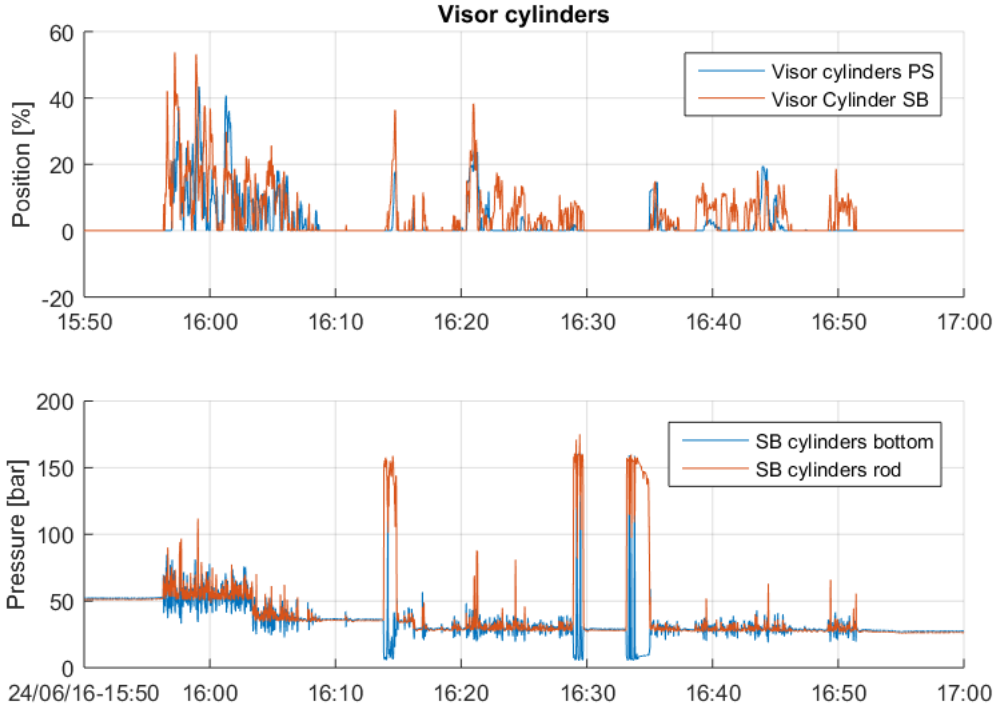


Figure 5.12: Visor cylinders position and pressure signals during dredging.

5.2.2 Estimation results on measurements

With the measurement data, the modelled trail force of the draghead on the starboard side is obtained. Since the pressure in the visor cylinders of the port side draghead is not measured, this modelled trail force can not be calculated. Therefore, the measurements of the force sensors on the port side suction tube are used for the estimator. With one modelled and one measured trail forces and the ship inputs and output signals from measurement data, the estimator is simulated. The variances in the R matrices are set equal to the variance on the noise which the output signals contain. They are equal to the variances as in Section 5.1. See Table 4.5 for the definitions of the states of the observer.

$$R = \mathbb{E}[vv^T] = \text{diag} \begin{bmatrix} 10^{-3} \\ 10^{-3} \\ 10^{-6} \end{bmatrix} \quad \text{with } y = \begin{bmatrix} SOG & [\text{m/s}] \\ COG & [\text{rad}] \\ \psi & [\text{rad}] \end{bmatrix} \quad (5.8)$$

The variances in the Q matrices are equal to the variances as in Section 5.1 as well. See Tables 4.4 for the definitions of the states of the observer. The initial state is chosen about equal to the expected real state. This is done by first simulating the estimator with higher variances on the current estimates for an aggressive convergence. The values of the current estimates are then used to initialise the estimator:

$$x_0 = \begin{bmatrix} .7 \\ 0 \\ 0 \\ 3.7 \\ 1 \\ 1 \\ 0.4 \\ 0 \end{bmatrix} \quad Q = \mathbb{E}[ww^T] = \text{diag} \begin{bmatrix} 10^{-7} \\ 10^{-8} \\ 10^{-9} \\ 10^{-12} \\ 10^{-7} \\ 10^{-7} \\ 10^{-8} \\ 10^{-8} \end{bmatrix} \quad P_0 = 1000 \cdot Q \quad \text{with } x = \begin{bmatrix} v_x & [\text{m/s}] \\ v_y & [\text{m/s}] \\ \psi & [\text{rad/s}] \\ \psi & [\text{rad}] \\ c_{F.sb} & [-] \\ c_{F.ps} & [-] \\ v_{cN} & [\text{m/s}] \\ v_{cE} & [\text{m/s}] \end{bmatrix} \quad (5.9)$$

With these settings, the estimator is simulated on the measurement data.

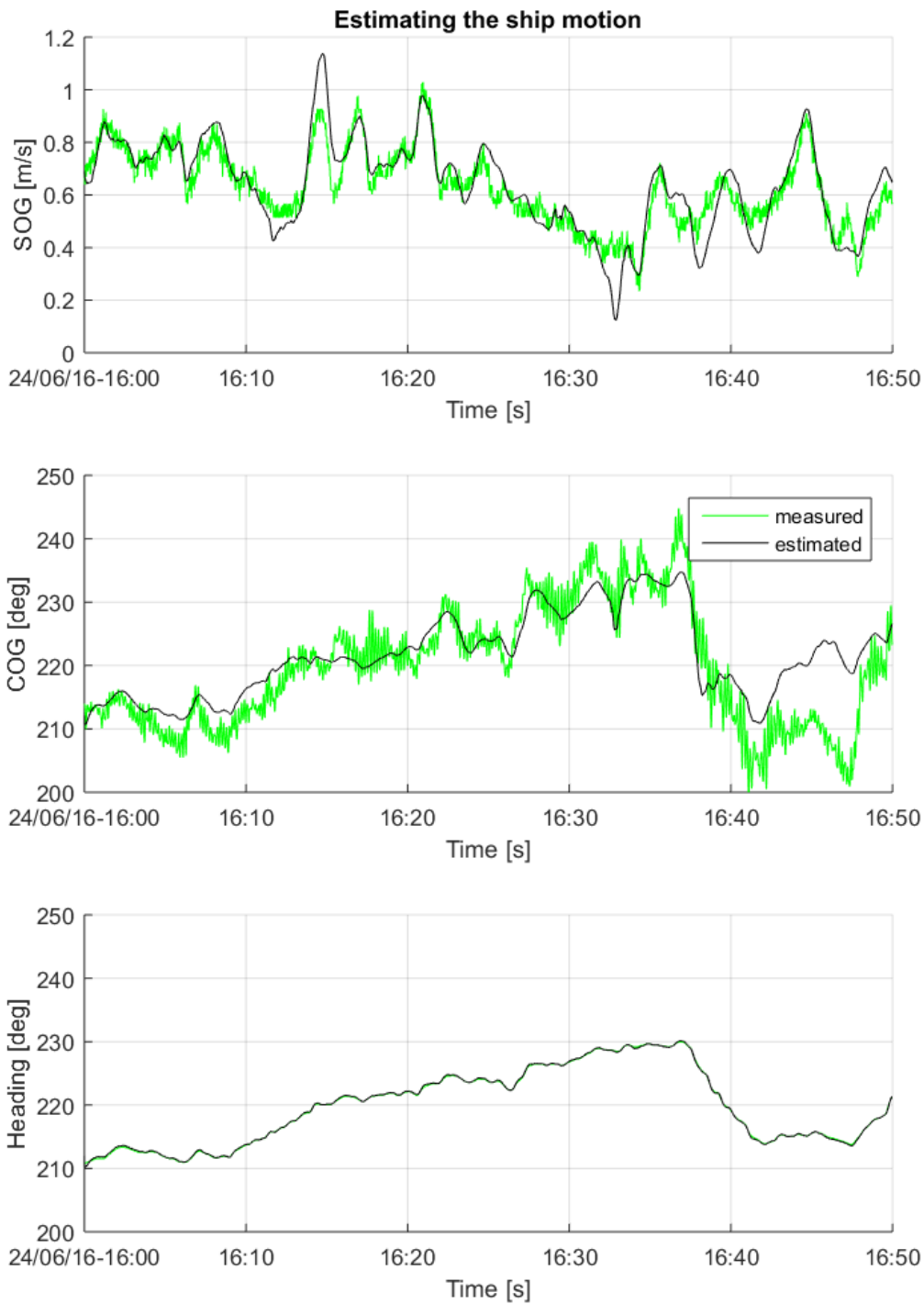


Figure 5.13: Ship motion estimations. Note that the estimation of the heading covers the measured signal because of the low noise.

Figure 5.13 shows that the estimated motion of the ship approaches the measurements well. This makes sense since they are all directly measured. Because of the low noise on the heading measurement, this signal is estimated accurately. The estimated speed over ground and the course over ground sometimes deviate from the measurements. This is because their variances are higher and the estimated trail force sometimes contains a large offset. The incorrect trail force is included in the prediction of the motion, which causes these offsets in the estimated ship motion. Furthermore, it shows that the propeller pitches (shown in Figure 5.11) are controlled manually which causes a fluctuating velocity of the ship.

Figure 5.14 shows the estimated trail force and current. Since the measured trail force of the port side is used for the estimator, this result is not shown. The modelled trail force of the starboard side contains significant offsets around 16:14, 16:29 and 16:34. This is because the visor is set to 'controlled mode' during these periods, as shown in Figure 5.12. Therefore, the force from the visor cylinder as obtained from the pressures is assumed to be negative, which results in a modelled cutting force equal to zero. Because of these offsets, the performance of the estimation reduces and the covariances of the state estimations increase. As a result, the estimator reduces the gain on this trail force and estimates more current coming from the front. During the time period as shown here, the ship is heading south-west (225°) so both the north and east components of the estimated are increased.

Because both a measured (PS) and a modelled trail force (SB) are used for the estimator at the same time, it is difficult to value the results. The correction gain of the PS trail force deviates from 1 but it is difficult to say if this is caused by an offset on the trail force measurement, by an inaccurate modelled trail force or by an inaccurately estimated current. It would be useful to have measurement data available from which both trail forces can be modelled. Furthermore, it is expected that the performance of the estimations increase when the modelled trail force contains less invalidities. This will be achieved when the visor is not positioned all the way down constantly. Despite the offsets, it can be concluded that the trail force and current can be estimated on measurement data.

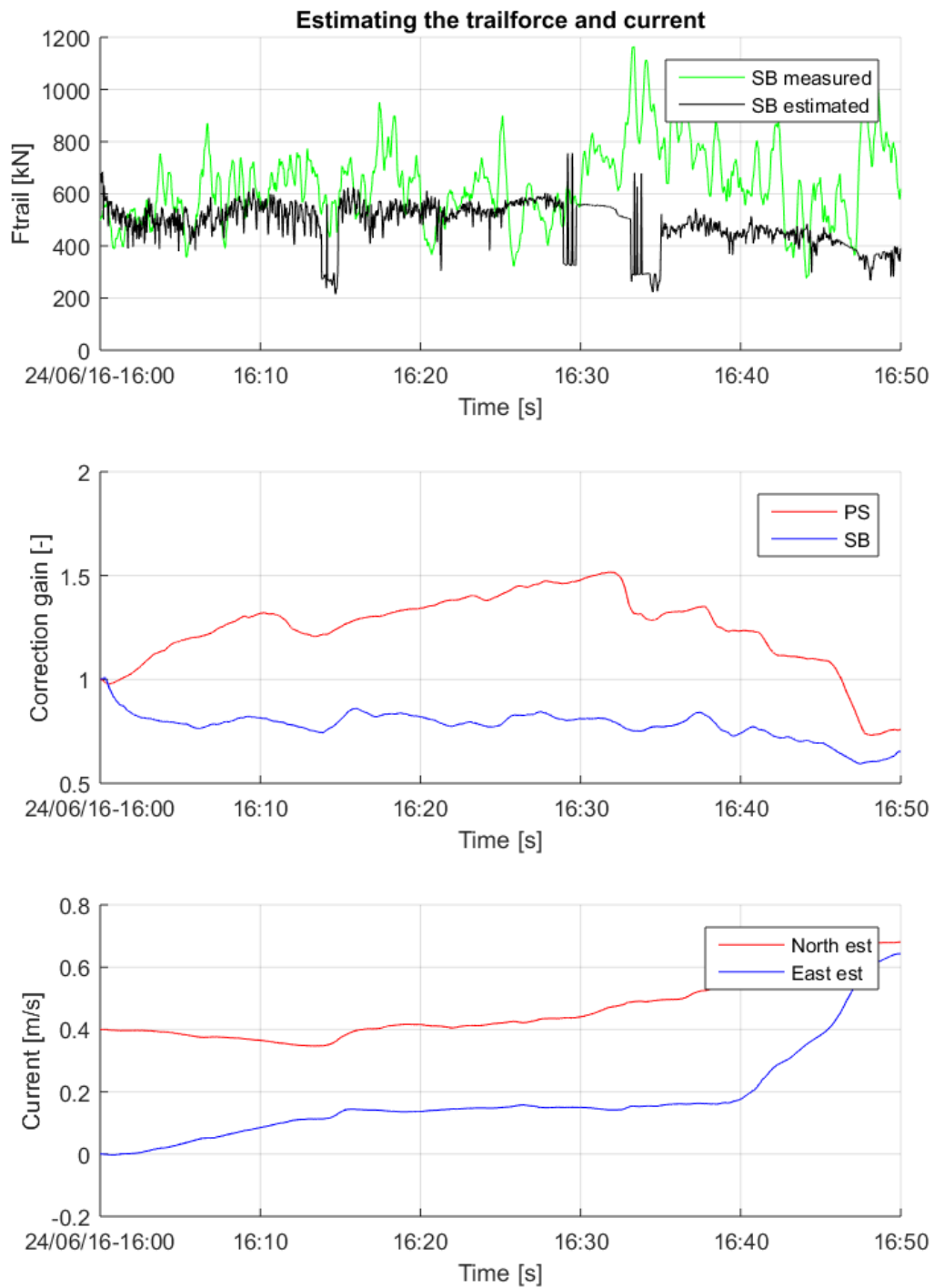


Figure 5.14: Trail force and current estimations.

Chapter 6

Conclusions and Recommendations

Trailing suction hopper dredgers (TSHD) are used for waterway maintenance and land reclamation. By trailing a draghead over the bottom, the TSHD excavates soil. Pulling the draghead's teeth through the sand causes a resistance, which is the major part of the trail force. The dynamic positioning system (DP-system) controls the motion of the TSHD during dredging. To optimize the dredging performance and efficiency, the ship must be kept at an optimal constant velocity. Because the trail force influences the motion significantly, it is important to know this disturbance so it can be directly compensated. The trail force is estimated because force sensors are expensive and fragile. In the current DP-system of IHC, the trail force is estimated using the pressure difference in the draghead. The estimation can be improved since more knowledge about the dredging processes is now available. Furthermore, the modern dragheads and suction tubes are equipped with more sensors which can be used as well.

6.1 Conclusions

In this thesis it is shown how the trail force and the current can be estimated for a TSHD. An estimator is built which uses a model of the ship dynamics and a model of the trail force. Chapter 3 shows how the models are obtained and validated using measurement data from a seatrial of the TSHD 'Jun Yang 1'. The trail force is modelled statically, using the following steps:

1. The cutting force is obtained by assuming the visor is in an equilibrium state. The visor cylinders, the visor's weight, the pressure difference in the draghead and the force of the soil on the teeth affect the rotation of the visor around the joint. By modelling all influences and assuming $\sum M = 0$, the moment of the teeth around the visor joint is obtained. Using the angle of the teeth and the cutting theory of Miedema [?], the horizontal and vertical components of the cutting force are approximated.
2. The friction force in the heel is obtained by assuming the lower suction tube is in an equilibrium state. The gravity, swell compensator, jets, differential pressure, cutting force and heel force exert a moment on the lower suction tube around the cardan joint. Using the assumption $\sum M = 0$ and the in (1) obtained cutting force, the moment of the heel friction at the cardan joint is obtained.
3. The horizontal components of the cutting force and the friction force in the heel are added up to model the trail force. This method is validated with measurements and it is shown that a VAF [?] of 92.5% is achieved.

The ship dynamics are modelled by deriving the thrust forces, drag forces and trail forces. All forces on the ship are obtained in the forward, sideways and rotational direction to model the ship motion.

Chapter 4 describes the estimator design. The estimator makes a real time estimation of the trail force and the current using the ship dynamics model and the trail force model. By combining information from the trail force model and the ship dynamics model, an estimation of the current and the trail force is made. The ship dynamics model in the estimator is a discretised state space system of the differential equations as described in Equations 4.13 - 4.14, using the Runge-Kutta 4 method. The estimator compares the measured ship outputs with the predicted motion from the ship dynamics model and the actuator signals, and estimates the trail force and the current. Because the model of the ship dynamics contains nonlinearities, the unscented Kalman filter is chosen as an algorithm for the estimator.

In Chapter 5, a test scenario was defined that represents realistic dredging circumstances. The estimator is tested in simulation, where the model as described in Chapter 3 is used to simulate the real process. It is shown that the trail force and current are estimated accurately. The trail force estimation has a VAF of 99% and a steady state error of 2%. Especially the slow dynamics are estimated accurately. The currently used method is simulated as well and achieves a VAF of 95%. Therefore, an improvement is shown using the trail force model for the estimator. The current estimation converges as well but contains a steady state error of 0.1 m/s. Measurement data from the seatrial is also used to test the estimator and it is shown that the estimator works. However, it is much harder to measure the performance of the estimator because the limited amount of suitable data. The reliability of the trail force measurements is limited and not all signals were available to model the trail force on the starboard side.

6.2 Recommendations

The estimator as presented in this thesis showed that it is able to estimate the trail force and current on data from simulations and measurements. The next step is to implement the estimator aboard a real TSHD and investigate the performance of the DP-system. The following recommendations are made regarding implementation:

- When the visor's cylinders are at their minimal or maximal positions, some assumptions made in the trail force model are not valid. This causes the modelled trail force to be inaccurate and degrades the performance of the estimator. The validity of the model can be detected by setting up conditions which will use the positions of the visor and the swell compensator. When the trail force model is not valid, the estimator should temporary fall back on the currently used method which uses a pressure difference based estimation.
- The estimator has difficulties in distributing the correct part of the total disturbance forces to the trail force and the other part to the current. This could be solved by having the current estimation converged before the dredging starts. When dredging, the current estimation can be slowed down so the estimator will focus on estimating the trail force. This method is already used in the DP-system.
- When the ship makes a turn, a small inaccuracy in the estimator's ship dynamics model arises. This causes an offset on the current and trail force estimates. It is expected that freezing the trail force and current estimation based on the heading rate of the ship will improve the accuracy of the estimations.

This thesis shows an improvement using the trail force model for the estimator. More improvements can be achieved by further research on the following subjects:

- When the heel is pushed hard on the bottom, bulldozing occurs. It is difficult to model or notice this process. Bulldozing affects the trail force significantly, so research on this will be valuable for improving trail force estimation. When a method is derived which notices bulldozing, the heel's friction coefficient in the model can be increased for example. This way, bulldozing is taken into account.
- The trail force model assumes that the position of the centre of pressure on the teeth is constant while cutting. However, this might not be the case, especially for dragheads with

two rows of teeth as used in this thesis. With a low visor, the last row of teeth will probably have higher cutting forces while a high visor will result in higher cutting forces on the first row of teeth. Investigating this effect is therefore recommended.

- When better trail force measurements are available, it is easier to validate models describing the thrust force, drag force and trail force. If the measurements have a good quality, they can even be used to fit the models which increases the accuracy of the models.
- When the wind is measured as well, this effect can be included. The wind was neglected in this thesis but it is expected that the estimator will perform better when this force is included.